Geophys. J. Int. (2008) **172,** 363–382 doi: 10.1111/j.1365-246X.2007.03647.x

Stochastic waveguide in the lithosphere: Indonesian subduction zone to Australian craton

B. L. N. Kennett[1] and T. Furumura[2]

[1] Research School of Earth Sciences, The Australian National University, Canberra ACT 0200, Australia. E-mail: brian.kennett@anu.edu.au
[2] Earthquake Research Institute, University of Tokyo, 1-1-1 Yayoi, Bunkyo-ku, Tokyo, 113-0032, Japan

Accepted 2007 October 2. Received 2007 October 1; in original form 2007 July 4

SUMMARY

Earthquakes occurring in the Indonesian subduction zone recorded in the cratonic regions of northern Australia have long, high frequency coda associated with both P and S waves. Similar behaviour is seen for earthquakes within Australia on paths within the cratonic regions. The complex character of the coda and its rapid spatial variation indicate that the high frequency waves have travelled within a zone of strong, multiple scattering with very high intrinsic Q. There are subtle variations in the nature of the coda that can be described through a coda Q. The variations in coda are associated with the position along the arc and the nature of the transition from the subduction zone to the continental lithosphere. The character of the coda observations can be captured with numerical simulations in models derived from seismic tomography for northern Australia and the neighbouring subduction zone, incorporating lower crustal and mantle heterogeneity with much longer horizontal than vertical correlation length. High frequency calculations to high frequency (16 Hz) for long propagation distances (up to 1500 km) have been carried out using finite difference modelling on the Earth Simulator. The variations in coda properties can be associated with the way in which the seismic energy gets ducted into the stochastic waveguide associated with the lithosphere. The most efficient transfer occurs where continental lithospheric material is adjacent to the earthquake zone.

Key words: Computational seismology; Guided waves; Wave scattering and diffraction; Wave propagation; Cratons; Australia.

1 INTRODUCTION

A characteristic feature of seismic events along the front of the Indonesian subduction zone recorded at stations in northern Australia is very long duration coda with high frequency content for P and S waves. Such records are very common at the Warramunga array (WRA) in northern Australia for events in front of the Banda Arc at about 13° epicentral distance (Kennett 1986), and indeed small Banda earthquakes ($Mb \sim 3$) can be recognized immediately by their high frequency coupled with the time separation between P and S waves (approximately 2 min), even though these events cannot be readily located. Similar characteristics are seen for earthquakes in Australia recorded on cratonic paths. The high frequencies persist for minutes and thus very high intrinsic Q is required in the propagation zone. The chaotic nature of the seismograms and strong variability between neighbouring sites indicate a very strong scattering regime (see, e.g. fig. 3 of Kennett 1987).

The detailed character of the seismic records show systematic variations with position along the Indonesian arc that can be associated with the varying structure adjacent to the subduction zone, in particular the configuration of Australian cratonic material. Both the character of the seismograms and the geographic variability can be captured by numerical simulations incorporating stochastic heterogeneity with aleotropic properties, so that the correlation length is much smaller in depth than in the horizontal direction.

2 OBSERVATIONS

Seismograms for waves traversing the Precambrian cratons of Australia from the Indonesian subduction zone show an extended coda of high frequency waves for both P and S waves. Commonly, the onset of the major phases is marked by a lower frequency arrival for both P and S, but within a second or two the high frequencies dominate and are sustained for minutes (Fig. 1). The seismograms have significant energy above 4 Hz and the rate of decay of this high frequency energy is slow for all components of motion, as can be seen from the frequency time analysis in Fig. 1.

As would be expected the initial onset of P shows negligible amplitude on the transverse component to the great circle path, but the high frequency arrivals are of similar amplitude on all three components. Such behaviour is what would be expected of an environment with intense multiple scattering and a very high intrinsic Q. The high frequency arrivals can persist to epicentral distances of 18° or more for paths within cratonic material. However, a moderate component of non-cratonic path on the continent is usually enough

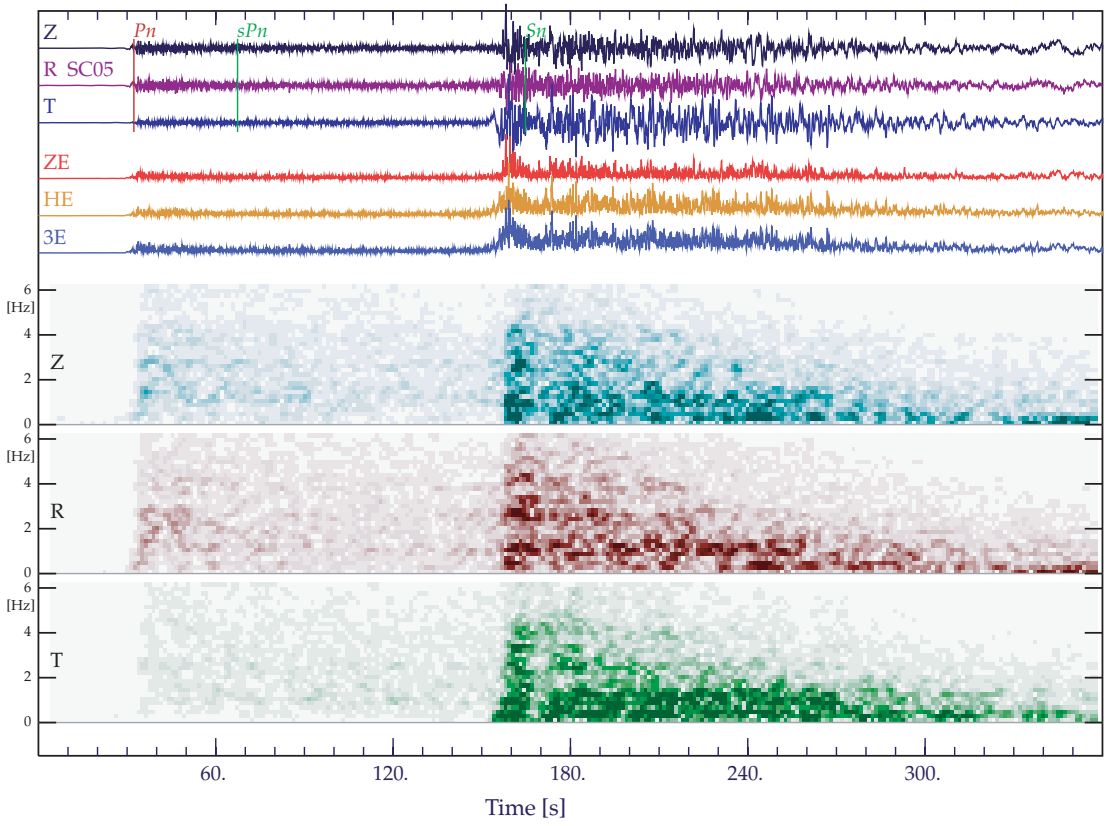

Figure 1. Three-component seismograms for an event in the Flores arc recorded at a portable broad-band station in the Northern Territory of Australia at an epicentral distance of 12.0°. The component triad in the upper panel is rotated to the great-circle between source and station. In the middle panel the vertical, horizontal and three-component energy contributions are shown. In the lower panel a frequency time analysis is performed for each component to show the slow decay of the high frequency energy for both P and S. The vertical lines indicate the arrival times predicted for the ak135 model (Kennett et al. 1995).

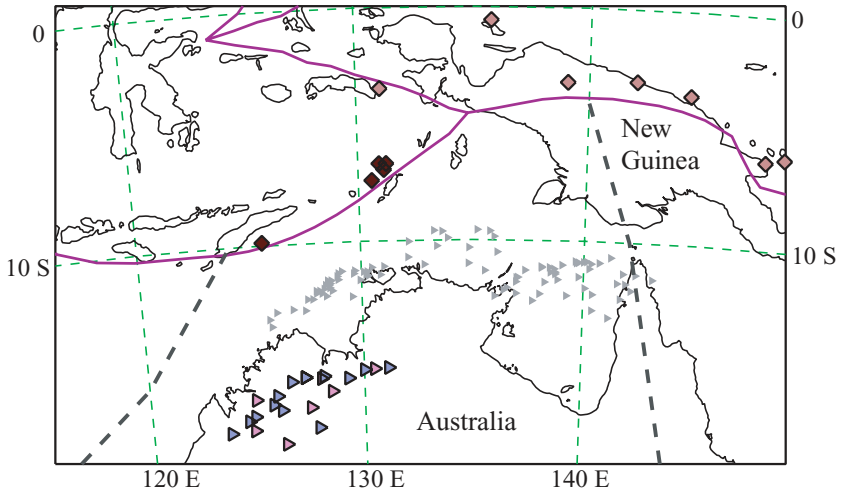

Figure 2. Locations of portable broad-band stations in the Kimberley region of northwestern Australia (triangles) and regional source through the Indonesian arc into New Guinea (diamonds). The midpoints of the wave trajectories are shown with triangles in tone. The approximate boundary of the North Australian craton is indicated by a heavy dashed line.

to suppress the high frequencies. The characteristic extended coda is seen for events down to 160 km depth but, as noted by Korn (1988) for short-period records at WRA, events deeper than 200 km have a shorter coda mostly likely generated close to the receiver. Propagation paths for such deeper events will largely lie outside the heterogeneous lithosphere.

A good example of the influence of propagation path is provided by seismic wave propagation to portable broad-band stations in the Kimberley region of northwestern Australia, during deployments in 1997 and 1998, from shallow events in the western end of the Indonesian arc into New Guinea (depth range 20–60 km). The configuration of sources and receivers are shown in Fig. 2, together with

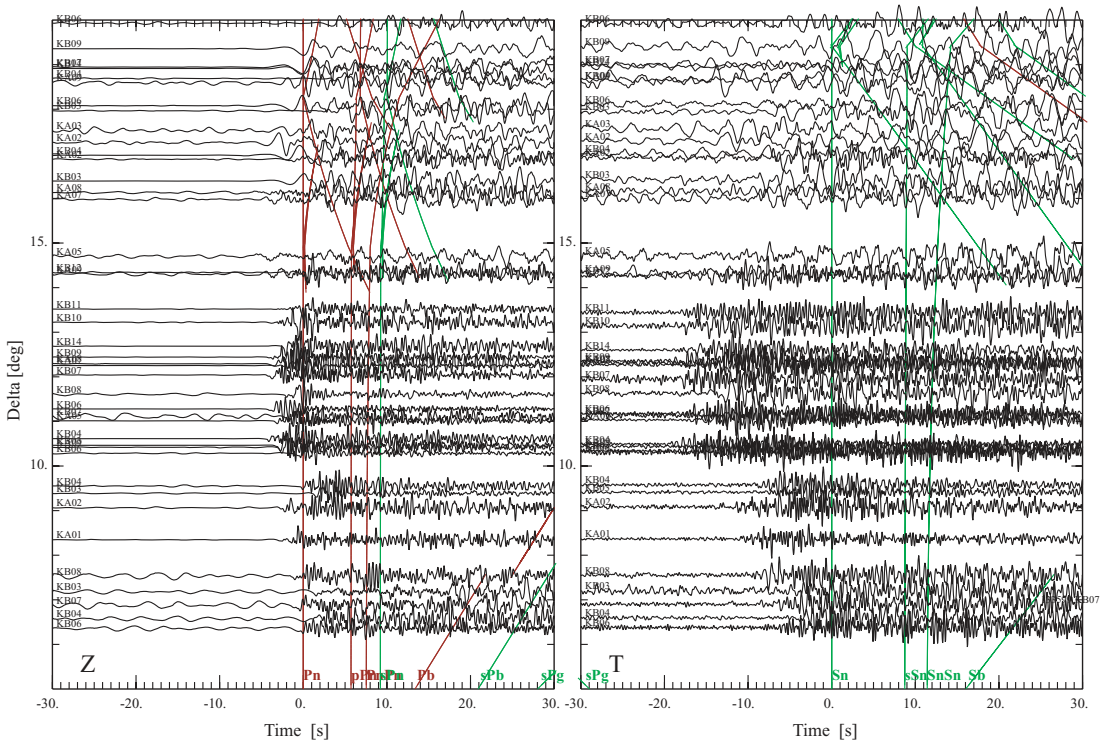

Figure 3. Broad-band unfiltered seismograms at the Kimberley stations from the events shown in Fig. 2. The traces in each window are aligned on the expected arrival times for P or S waves for the ak135 model (Kennett et al. 1995) for a 25 km depth event. Depth corrections are applied separately to the P and S waves to correct the events to a common depth. Vertical component records are shown for the P wave window and the transverse component for the great circle path for the S-wave window. The relative traveltimes for other phases for a 25 km deep source in the ak135 model are superimposed on the traces; phases leaving the source as P are shown in red, and as S in green.

the approximate outline of the Australian cratonic material and the midpoints of the paths. All the sources are well located, with magnitude of 5.2 or greater, and CMT solutions in the Harvard catalogue. Those sources which provide the strong high-frequency coda at the Kimberley stations are indicated with darker symbols. Events on the farther side of the Banda Sea have a strong influence from the structure behind the arc and show very little high frequency energy at the Australian stations. The events in northern New Guinea with epicentral distances beyond 15° also do not give high frequency arrivals to the Kimberley stations. However, there are some examples of such high frequency arrivals for similar events in Irian Jaya to stations further east within the craton, where the paths are nearly north–south.

Record sections of both the P and S arrivals in Fig. 3 at the Kimberley stations for the events mapped in Fig. 2 show pervasive high-frequency arrivals with a long duration of coda out to 15°. Events at greater distances lie outside the cratonic zone. The seismograms in Fig. 3 are aligned on the expected arrival times for P and S for the ak135 model (Kennett et al. 1995) that represents a continental average. The paths from the Indonesian arc into the North Australian craton are fast for both P and S compared with ak135. The advance of the S arrivals relative to ak135 approaches 20 s between 10° and 15° epicentral distance, even though the advance of the P waves is only of the order of 6 s. These large negative residuals from ak135 are not due to source mislocation, but a consequence of lithospheric structure. Very high S wave speeds have been mapped in both body- and surface-wave tomography for northern Australia (see, e.g. Kaiho & Kennett 2000; Fishwick et al. 2005), with deviations of 6 per cent or more from ak135 in the depth range from 75 to 150 km.

In Fig. 4 we display the three-component records for a single event in the Banda arc for stations in the epicentral distance range from 8.3° to 12.3°. The records are normalized to the maximum energy of ground motion within the time window, so that all three components at each station are on the same scale. Once again we show a window of one minute around the expected arrival times of P and S. Although all the records for both P and S waves show strong high-frequency content, there is considerable variation between the nature of the seismograms at the different stations, even for stations at very similar epicentral distance. Nevertheless, in each case we see a distinct frequency separation between a low-frequency onset and the high frequency train that we would associate with scattering. As noted above, the low-frequency P wave onset is missing on the transverse component, but the high-frequency energy starts at the same time as for the vertical and radial component and tends to increase in amplitude as time progresses. For the S arrivals, the amplitude of the high-frequency arrivals is comparable on all three components.

The behaviour illustrated above is not confined to a single group of paths, and is indeed characteristic of events from 100°E to 136°E at stations in the cratonic regions of Northern Australia. Fig. 5 shows a record section for a single event at the front of the Java arc recorded by a network of portable broad-band stations in northwestern Western Australia. The stations span the epicentral distance range from 9° to 16°, with the first 6° crossing oceanic lithosphere before entering the submerged continental material of the Northwest Shelf. The radial and transverse horizontal components to the great circle between source and receiver are shown. Both the P and S waves are markedly fast compared with the predictions from the ak135 model. Although the seismograms have a similar general character,

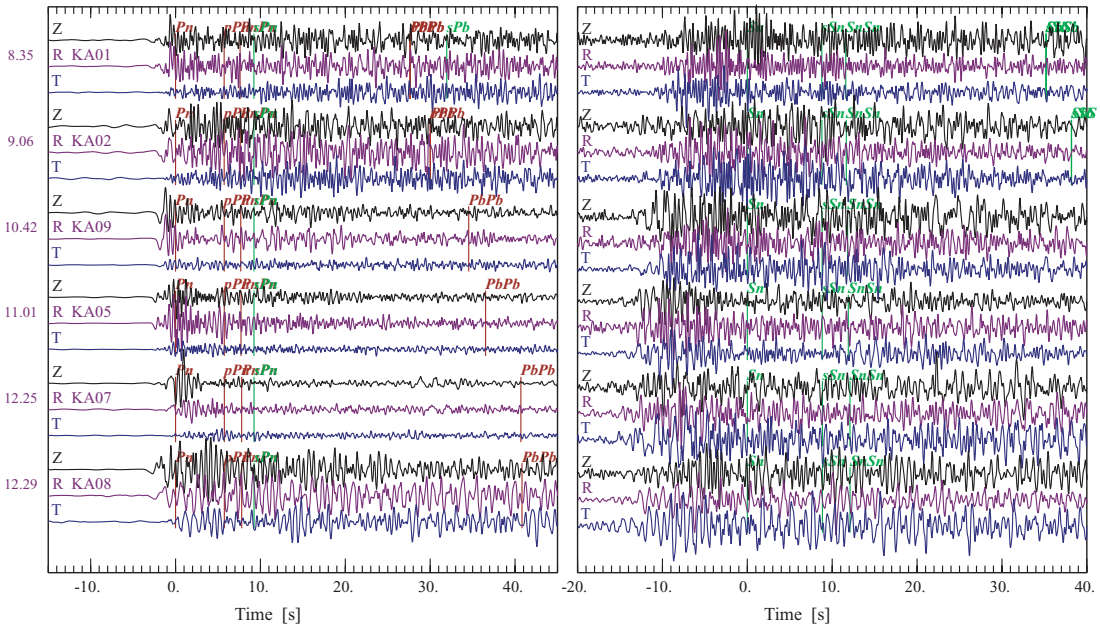

Figure 4. Three-component triads of unfiltered broad-band records for an event in the Banda arc (1997:239:09, −7.36°S 130.59°E, 30.0 km depth) recorded across a network of stations. The epicentral distances for each trace are shown to the left. The traces in each window are aligned on the expected arrival times for P or S waves for the ak135 model. Each triad is normalized by the maximum energy in the time window.

there are notable differences between stations at similar distances, even though there is a very narrow range of take-off angles from the source. The low frequency onset for P is prominent on the further stations, but very soon after this arrival the amplitude of the high-frequency wavetrain is comparable on the radial and transverse components. The more distant stations CP08–CP14 lie within or beyond the Proterozoic Capricorn orgenic belt, rather than the Archaean Pilbara craton on which the northern stations sit, yet there is little change to the character of the coda for either P or S waves. It would appear that the mantle lithosphere is playing a significant role in imposing the properties of the high-frequency waves.

The intrinsic Q for paths in the Australian cratonic lithosphere are very high, as noted by Gudmundsson et al. (1994), and it would appear that the high-frequency scattered waves are ducted within this high Q environment. As we can see from the examples in Figs 1, 3 and 4 there is very little difference in frequency content between P and S and so the differential attenuation δt^*_{SP} between these phases will be small. Fig. 6 displays all paths from regional events into portable broad-band stations in Australia that have $\delta t^*_{SP} < 0.2$. More than 1000 paths show very low differential attenuation between S and P, and the majority of these paths extend from events in the Indonesian arc into stations in northern Australia. A few events in the Australian continent, which have been captured by temporary stations. show similar character. Almost all of the high Q paths have a significant cratonic component, and have associated P and S coda with a long duration of high-frequency energy.

Although the general features of the seismograms are similar, there are systematic differences in behaviour depending on source location that appear to be related to the configuration of the Australian cratonic lithosphere relative to the subduction zone. Such variations can be recognized through the sustained profile of the envelope of the high frequency arrival for both P and S waves. The considerable variations in the nature of the transition from the thick Australian lithosphere and the subduction zone beneath the Indonesian arc are illustrated in Fig. 7 with north–south sections through the P wave tomography model of Widiyantoro & van der Hilst (1996). In the west (zone A—120°E), the thick lithosphere has not reached the subduction zone and the lithosphere necks into a distinct oceanic zone that is now being subducted. In zone B (124°E) the thick Australian lithosphere has nearly reached the trench, but there is a distinct thinning into the oceanic material, with active subduction. At zone C (128°E) the Australian lithosphere has arrived at the arc and subduction has ceased, even though there is remnant subducted material. To the east in zone D (131°E) the Australian lithosphere appears to abut the material in which earthquakes are occurring, with direct transmission into the lithosphere and very strong, complex signals.

The rate of decay of the high frequency components can be described by a simple coda-Q model for which the amplitude at frequency f as a function of traveltime T is represented as (Xie & Nuttli 1988)

$$A \propto T^{-\nu} \exp(-\pi f T / Q_c). \quad (1)$$

Here ν describes the geometrical spreading of the waves, and T is the traveltime for the relevant wave type with appropriate coda Q_c.

For crustal studies, particularly the analysis of Lg attenuation, the exponent ν has typically been taken as 5/6, based on the model of an Airy phase in the crust. Hitherto there has been little analysis of distances beyond 1000 km, where there must be a significant component of propagation within the lithospheric mantle. The frequency decay of the power spectral density is illustrated in Fig. 8 for the seismogram shown in Fig. 1. The patterns of relative decay as a function of frequency and time can be well represented with $\nu = 2/3$ and $Q_c > 1500$. With such high coda Q it is difficult to get any control on possible frequency dependence of the coda Q. Comparable results are found for the different paths, although as noted above the envelope of the amplitude pattern varies before a systematic coda decay is established.

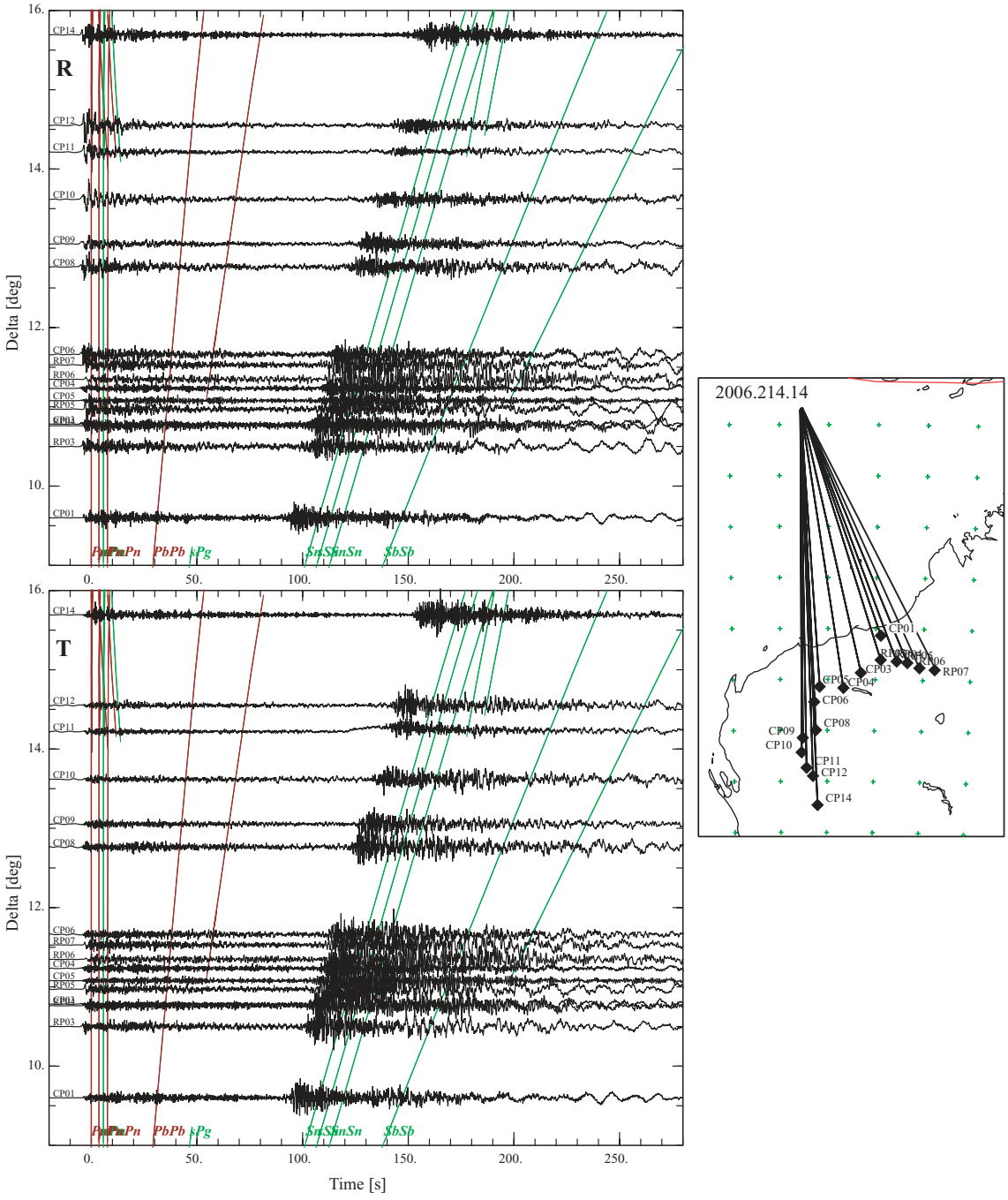

Figure 5. Record sections of radial and transverse component seismograms for a shallow event (15 km deep) at the front of the Java trench (−11.17°S 116.85°E) recorded across a network of portable seismic stations in northern Western Australia as shown in the map insert to the right. The seismograms are aligned on the expected P arrival times for the ak135 model, and the time trajectories of other phases are indicated. The ground velocity traces are unfiltered and normalized with respect to the three-component energy in the 5 min window.

3 NUMERICAL MODELLING OF SEISMIC WAVE IN AUSTRALIAN LITHOSPHERE

We illustrate the way in which high-frequency waves are guided into cratonic Australian lithosphere from the Indonesian subduction zone, using simulations of seismic wave propagation in heterogeneous structure with a 2-D finite-difference method (FDM).

The 2-D model is taken along a profile cutting from the Banda Sea to Australia through the broad-band seismic station at WRA, nearly perpendicular to the Indonesian subduction zone. The physical parameters for the crust and upper-mantle structure for Australia are based on the nip3 Australian standard model (Gudmundsson et al. 1994, Fig. 9, dashed lines). Earth flattening is applied to the model of P and S wave speed (V_p, V_s) (see, e.g. Kennett 1983, Chapter 1) in order to include the effect of the sphericity of Earth in a Cartesian-coordinate system, so that the model can be used with a conventional FDM grid (Fig. 9, solid lines).

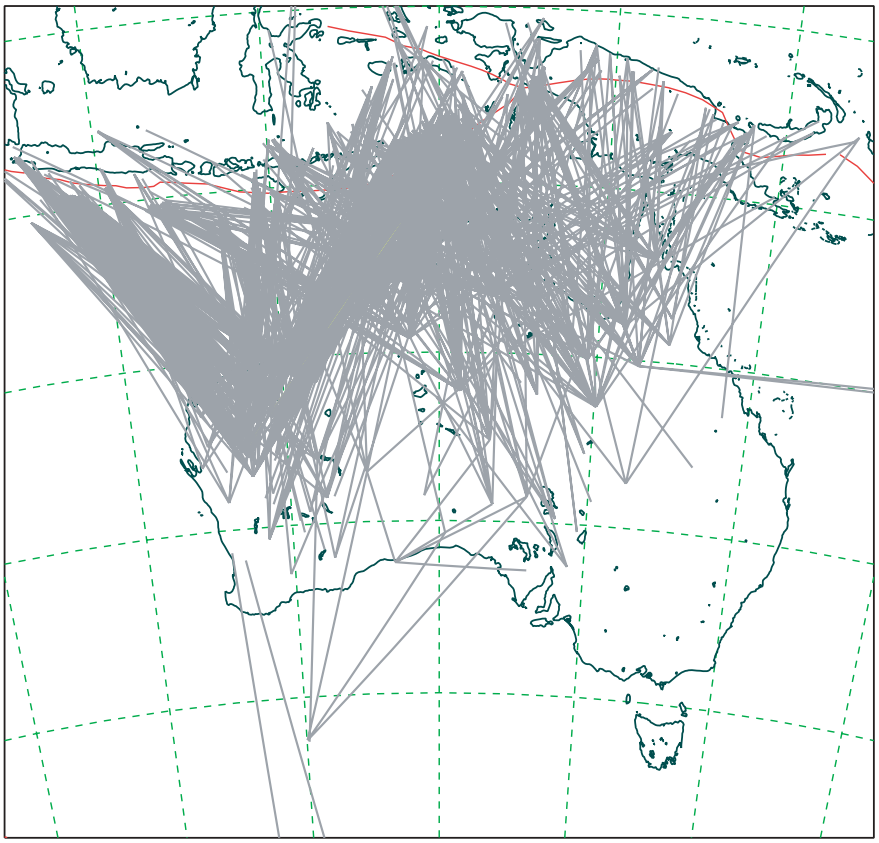

Figure 6. Paths with very small differential attenuation $\delta t^*_{SP} < 0.2$ determined from the spectral ratio of S and P waves. Most of these paths traverse the cratonic regions of Australia and display the characteristic long and high-frequency P and S coda displayed in earlier figures.

The 2-D model used for the simulation covers a region of 1800 km horizontally and 380 km in depth, discretized with a uniform grid interval of 0.0625 km in both directions (Fig. 10). The model is based on the P-wave tomography study of Widiyantoro & van der Hilst (1996) for region B (Fig. 7). The velocity model within the subduction zone component is similar to that employed by Furumura & Kennett (2005). A group of modified models have also been considered derived from the results shown in Fig. 7 at different positions along the arc (A,C,D).

A double-couple line source for a shallow-angle reverse fault event (dip 30°) has been placed inside the subducting slab 5 km below the top of the plate at a depth of 120 km. The high-frequency seismic wavefield (above 1 Hz) is not very sensitive to the details of the source mechanism, since multiple scattering of seismic waves in heterogeneous crust and upper-mantle structure disrupts the original four-lobe pattern of P and S wave radiations rather dramatically. The seismic source-slip function is a pseudo-delta function which radiates seismic waves with a maximum frequency of 16 Hz. The simulated seismograms are finally convolved with a suitable source slip-velocity function for the desired earthquake magnitude.

To achieve the long distance propagation at high frequencies (16 Hz) a parallel implementation of the FDM is employed in a staggered-grid configuration with 16th-order accuracy in space and second-order accuracy in time (Furumura & Chen 2004). The high spatial accuracy allows stable calculations for several thousand wavelengths at the highest frequencies. Frequency independent intrinsic anelastic attenuation for P and S waves (Q_p, Q_s) is introduced into the FDM simulation using the memory variable technique of Robertsson et al. (1994). Artificial reflections from the model boundaries are suppressed by employing a conventional absorber developed by Cerjan et al. (1985) that is applied in a 20-gridpoint zone surrounding the model.

The heterogeneities in the model are represented through a a von Karmann distribution with a Hurst number of 0.5, and variable correlation lengths in the horizontal and depth directions. This distribution includes short wavelength components but with a relatively rapid drop off in the heterogeneity spectrum. Heterogeneity is introduced in to the P wave speed, S wave speed and density with an assigned standard deviation for the fluctuations.

We have used very fine grid spacing of 0.0625 km in the FDM simulation, so that there will be adequate sampling for heterogenities with scales larger than 0.125 km. There could be some minor error associated with features with very small scales but the power in such small scale heterogenities would be very small. The shaping of the source signal applies a low pass filter to the results of the 16th-order staggered-grid FDM simulation and has the effect of suppressing the very highest frequency components where the representation might not be adequate. The practical frequency range in the seismograms displayed reaches 10 Hz.

The parallel FDM simulation was conducted using 32 nodes (256 vector processors) of the Earth Simulator supercomputer at the Japan Agency for Marine-Earth Science and Technology (JAMSTEC) in Yokohama. Each run required a CPU time of 5 hr with a computer memory of 0.64 GB to calculate 510 s of wave propagation using 510 000 time steps.

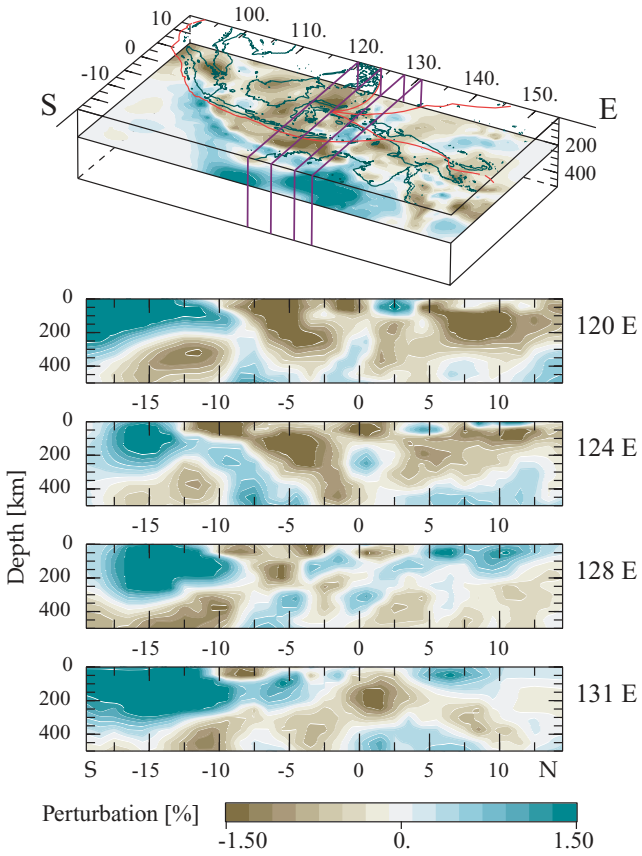

Figure 7. Cross-sections through the P-wave tomographic model of Widiyantoro & van der Hilst (1996) for the Indonesian region, displayed as deviations from the ak135 reference model. The locations of the sections are indicated in the key map above.

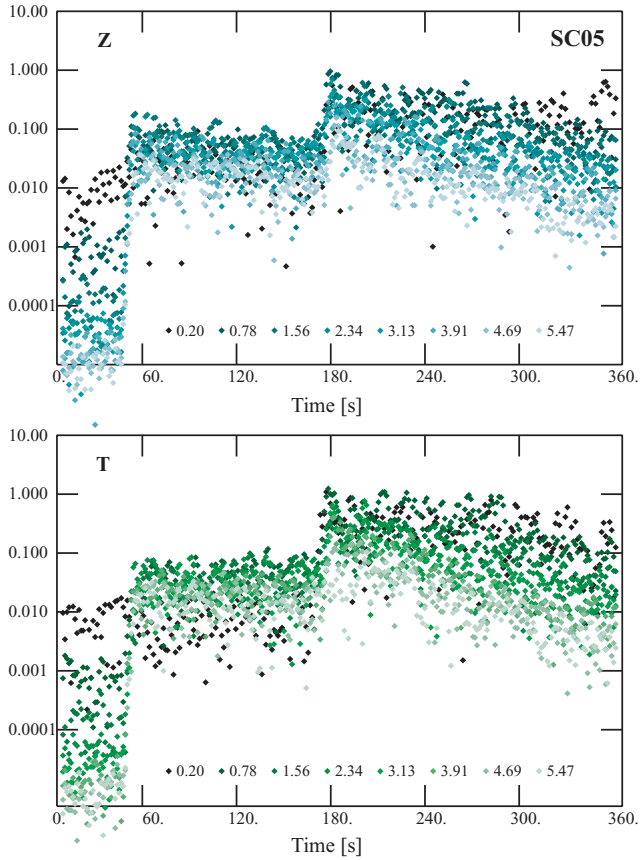

Figure 8. The variations of the power spectral density in the seismogram shown in Fig. 1 as a function of frequency and time. The vertical (Z) and transverse (T) components are shown, and soon after the P arrival the energy on the transverse component approaches that on the vertical for the higher frequencies. The symbols grade to lighter shades as the frequency increases as indicated in the key at the base of each panel.

3.1 Base Australian craton model

The first group of simulations employs a structural model of Australian lithosphere extending to the Indonesian subduction zone with the geometry illustrated in Fig. 10. Attenuation studies of the northern Australian region (Gudmundsson et al. 1994) show that the loss in the Australian Lithosphere is very low, but beneath the asthenosphere has rather low Q. Accordingly high-Q values are assigned for P and S waves in the lithospheric mantle and subducting slab ($Q_p = 2400$, $Q_s = 1200$) and craton ($Q_p = 1600$, $Q_s = 800$) to a depth of 200 km below Australia, and somewhat smaller values are used for the crust ($Q_p = 600$–800, $Q_s = 300$–400). Stronger attenuation ($Q_p = 120$, $Q_s = 60$) is assigned to the wedge mantle above the plate on the forearc side of the Indonesian subduction zone, compared to the uppermost mantle below the craton ($Q_p = 400$, $Q_s = 200$).

We introduce stochastic random heterogeneity in the lithosphere for both crust and mantle structure with fluctuations of V_p, V_s and density (ρ) that enhance the scattering of high-frequency signals, and leads to long P and S wave coda as observed in broad-band seismograms in the inland of Australia. Dominant small-scale heterogeneities in the crust and upper-mantle structure have recently been investigated for long-range exploration experiments in different areas such as in Europe (e.g. Nielsen et al. 2003) and have been proposed as the cause of large Pn and Sn signals with long coda. Furumura & Kennett (2005) have demonstrated that horizontally elongated properties for the heterogeneities ('quasi lamina structure') in the crust and mantle can produce significant forward scattering of high-frequency signals and thus an effective stochastic waveguide for high-frequency signals. Such models provide a good representation of the high frequency arrivals at stations above subduction zones for intermediate and deep earthquakes (Furumura & Kennett 2005, 2008).

We model the distribution of random heterogeneities in the crust and mantle with a von Karmann distribution function with aeolotropic correlation properties: an elongated correlation distance ($A_x = 5$–20 km) is applied in the horizontal direction compared with a much shorter correlation distance ($A_z = 0.25$–0.5 km) in depth/thickness. The standard deviation of the variations from the background model σ is set at 1–2 per cent, based on the results of recent studies regional high-frequency seismic wavefields and numerical simulations (e.g. Nielsen et al. 2003; Furumura & Kennett 2005). The properties of the base model are summarized in Table 1. The attenuation for S waves is set at twice that for P waves, so $Q_\beta = Q_\alpha/2$.

3.1.1 Snapshots of the seismic wavefield

The results of the FDM simulation of the seismic wavefield for the base model are illustrated in Fig. 11 with snapshots of the seismic wavefield at T = 20, 80, 140, 200 and 260 s from the earthquake initiation, and with synthetic seismograms in Fig. 12. To achieve a clear representation of the P and S waves in the heterogeneous

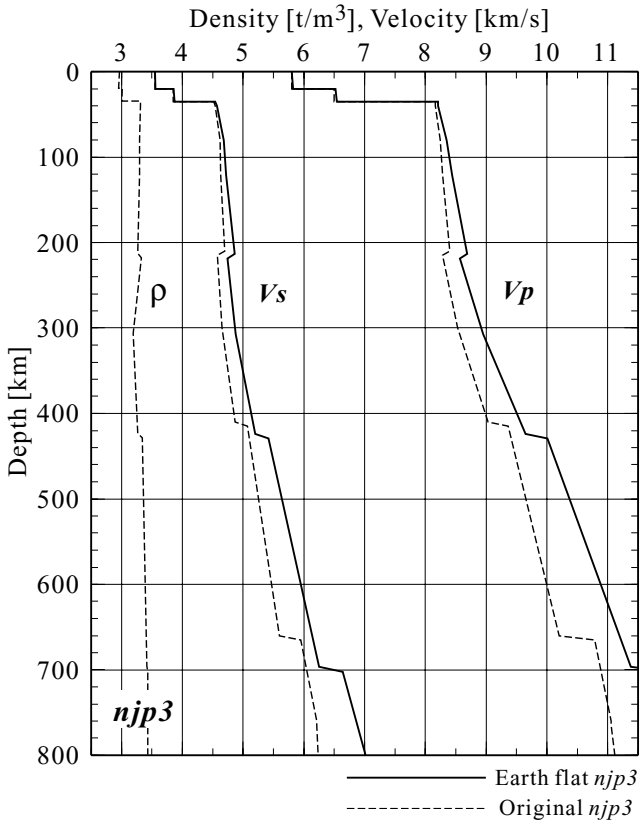

Figure 9. The depth variation of P- and S-wave velocity and density of Australian lithosphere (njp3; dashed lines) used in the 2-D numerical modelling and modified V_p and V_s by using the Earth flattening technique (solid lines).

structure, the simulated wavefield for the snapshots is separated into P and SV wave contributions by taking the divergence and curl of the 2-D wavefield. The contribution from the P waves is shown in red and that from SV waves in green.

In the first frame of the snapshots (T = 20 s, Fig. 11), the P and S waves radiating from a double-couple source in the subducting plate at 120 km depth show nearly spherical wavefronts for the P and S waves travelling upward in the subducting slab and penetrating into the surrounding mantle. Significant scattering of high-frequency seismic waves in the heterogeneous subduction zone structure and internal heterogeneities in the subducting plate modify the radiation pattern of P and S waves into a nearly isotropic distribution.

As time progresses the P and S waves travelling into the high Q Australian lithosphere develop a thick band of P- and S-wave coda by the action of multiple scattering of seismic waves caused by the internal heterogeneities. The configuration of the wavefield in the various snapshot frames indicate that the dominant processes are P-to-P and S-to-S scattering. Conversions between P and S waves are of lesser importance except for the large P-to-S conversion at the free surface. Some seismic energy comes through the mantle into the Australian cratonic lithosphere through the tilted wall of the craton in the distance range from 200 to 400 km, and also contributes to the long P- and S-wave coda.

In the T = 80 s frame the mantle Pn signal is the dominant feature accompanied by a larger pPn signal both propagating through the middle of the frame at an apparent speed of about 9.0 km s^{-1}. The sPn signal converted from the S wave at the free surface has large amplitude (despite attenuation in the mantle wedge), and begins to separate from the Sn waves, arriving between the Pn and Sn waves in the middle frame (140 s). The multiple PmP and SmS reflections within the crust are the most prominent feature in the regional wavefield leading to a very long coda within the crustal waveguide. The long wavetrain of PmP and sPmP signals extends over a distance span of 1000 km in the crust beneath Australia and the tail of the P wave coda almost covers the later S wave signal.

The S waves have a much shorter wavelength than P waves and this leads to striking scattering and the accumulation of a long coda to the wavefront, associated with the stochastic waveguide formed by the heterogeneous Australian cratonic lithosphere (see 200, 260 s frame Fig. 11). The S waves are well trapped within the quasi-lamina structure by multiple reflections between the heterogeneities, but P-wave energy is gradually lost by conversion to S waves in such multiple internal reflections.

Table 1. Stochastic properties of base model.

Layer	A_x (km)	A_z (km)	σ	Q_α
Upper crust	5.0	0.25	2 per cent	600
Lower crust	5.0	0.25	2 per cent	800
Mantle 1	20.0	0.50	2 per cent	2400
Mantle 2	20.0	0.50	1 per cent	1600
Mantle 3	–	–	0 per cent	400

3.1.2 Synthetic seismograms

Synthetic seismograms for the radial- and vertical-components of ground velocity are displayed in Fig. 12 for stations in the epicentral distance range from 700 to 1500 km. An expanded version of the initial P-wave arrival is shown in the lower panel for each component. Each seismogram trace is multiplied by the square root of the epicentral distance, so that the geometrical spreading effect of body P and S waves from the 2-D line source are roughly compensated.

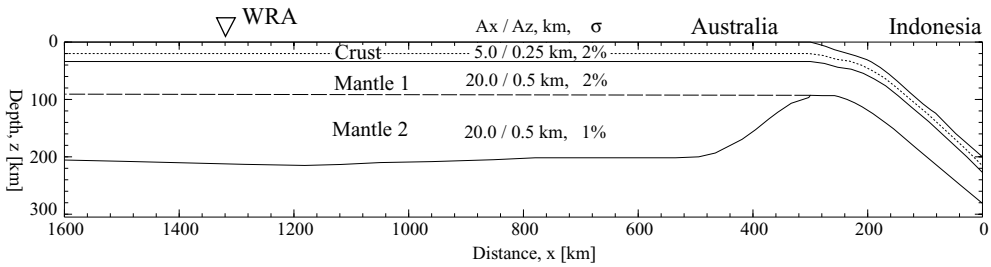

Figure 10. Model configuration for numerical 2-D FDM simulations representing a cross-section from the Australian lithosphere to the Indonesian subduction zone; random heterogeneities in the crust and mantle are specified in terms of the fluctuations with a characteristic scale (correlation length) in horizontal (A_x) and vertical (A_z) directions and standard deviation (σ) in each layer.

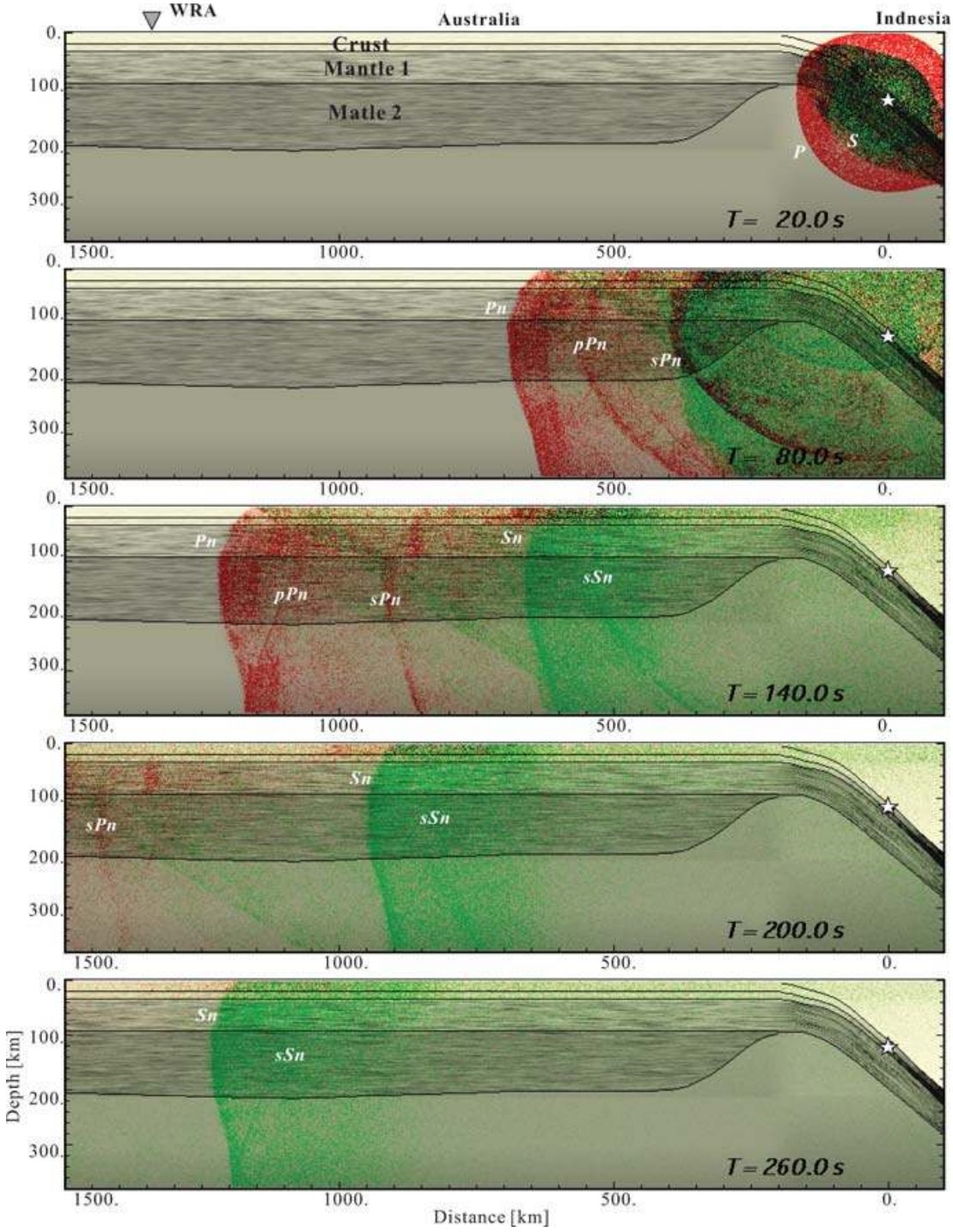

Figure 11. Snapshots of the seismic wavefield showing the P (red) and SV (green) contributions to the wavefield in the Australian lithosphere produced by a source in the Indonesian subduction zone at 120 km depth. Major seismic phases are indicated.

The waveforms are then convolved with a triangular source-slip function with a pulse width of $T = 0.2$ s assuming a source-slip history for a M5 source.

The development of a long tail of high-frequency P- and S-wave coda following the large Pn and Sn waves from the propagation of the wavefield in the heterogeneous lithosphere is clearly demonstrated in the seismograms shown in Fig. 12. The onset of Pn and Sn are lower frequency but almost immediately large amplitude arrivals with higher frequencies dominate. The time sequence at each site mirrors the behaviour seen in the snapshots in Fig. 11, the coda persists whilst the scattered wavefield sweeps past the observing site. The attenuation of the seismic signals through the high Q Australian cratonic lithosphere is rather weak, so that high frequency signals can be ducted to large distances.

Even for the shorter epicentral distances (700 km) the duration of the P- and S-wave coda exceeds 60 s induced by the presence of the zones of heterogeneity in the crust and mantle structure. Further the waveforms at neighbouring stations show a strong variation in

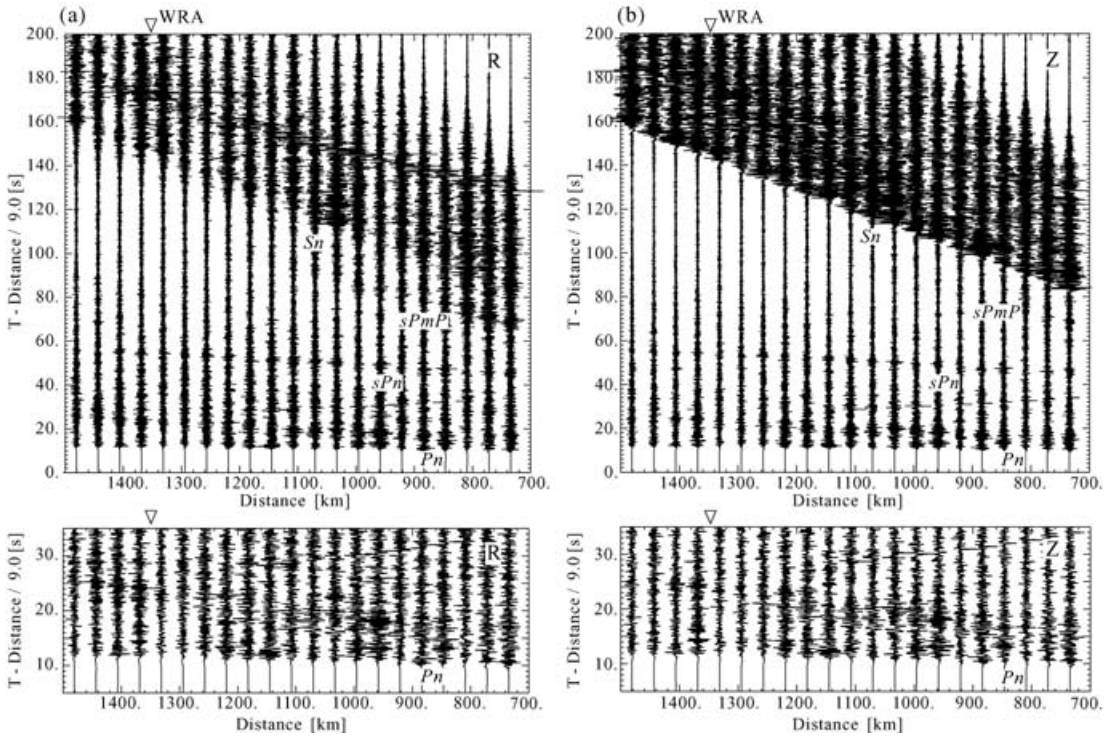

Figure 12. Synthetic seismograms for the radial (R) and vertical (Z) components of ground for stations in the epicentral distance range from 700 to 1500 km. An expanded view of the first 30 s of the P-wave contribution for both R and Z components is shown in the lower panel.

waveform as a result of strong multiple scattering, especially for high-frequency waves, a feature that is in common with the observations.

In the lower panels of Fig. 12, the P wave portion of the seismogram is displayed on an expanded timescale. The onset of the P arrival shows low-frequency signals ($f < 0.25$ Hz) signals followed by the high-frequency main arrival ($f > 2$ Hz) with a long coda. The time interval of one to two seconds between the low frequency onset and the higher frequency train for an epicentral distance of about 1300 km correlates well with the observed seismograms shown in Figs 1, 3–5. Such a separation in the low- and high-frequency signals is produced in the quasi-lamina structure due to the delay of most of the high frequency part of the P-wave signals due to multiple scattering from the internal heterogeneities, while the low-frequency waves with longer-wavelength tunnel through such structure to behave like a refracted head wave propagating through high-velocity layer (Fuchs & Schulz 1976; Furumura & Kennett 2005). Thus the separation of low- and high-frequency signals for the Pn phase observed in the broad-band seismograms and in these simulations support the concept of a quasi-lamina small scale structure in the Australian lithosphere.

3.2 Effect of heterogeneities in the crust and in the mantle

In order to find out how the random heterogeneities in the crust and mantle structure can contribute to the development of long and large P- and S-wave coda, we conduct a set of simulations using the same basic structural model, but with different patterns of heterogeneity distributions in each part of lithosphere.

Fig. 13 compares snapshots of the seismic wavefield for a common time frame of $T = 160$ s for the same class of source at 120 km depth with different class of heterogeneities. Model (a) has no random heterogeneity; model (b) includes just crustal heterogeneity, model (c) has heterogeneity in just the mantle layer 1; model (d) has heterogeneity throughout the mantle lithosphere and model (e) is the base model with full heterogeneity. A comparison of the set of synthetic seismograms for each of the models at a common station at an epicentral distance of $D = 1350$ km (equivalent to WRA from Banda Sea events) is displayed in Fig. 14.

For the homogeneous model (a) without any stochastic random heterogeneities in the crust and upper mantle, there is a clear pattern of successive P- and S-wave reflections from the Moho and the mid crustal interface (Conrad) coupling into the thick Australian lithosphere. The result is a somewhat artificial waveform for the seismogram (Fig. 14a) with many distinct pulses. The Sn arrival is rather weak and the duration and character of the coda of the P- and S-waves are very different from the observations. Simple modifications of the present model such as, for example, a change in shape of the boundaries or the V_p, V_s and Q parameters in each layer of the model, do not make much modification to the nature of the coda.

Once we introduce stochastic random heterogeneities into the crust extending from the Australian continent to the subducting plate in model (b), the scattering of seismic waves in crustal heterogeneities gives rise to the development of high-frequency P- and S-wave coda (Fig. 13b). However, the snapshots of the seismic waves and the synthetic seismograms in Fig. 14(b) show very weak Pn and Sn signals travelling in the lithosphere. The attenuation of the seismic waves is very striking with leakage of seismic energy into the deeper mantle from the bottom of craton. The relatively thin crustal zone of about 35 km thickness is not sufficient to sustain high-frequency seismic energy for more than 1000 km in the Australian continental lithosphere. A similar pattern is found when we introduce stochastic random heterogeneities in the mantle in the depth range between 35 and 80 km, model (c) with a homogeneous crust (Figs 13c and 14c). The slightly thicker stochastic waveguide

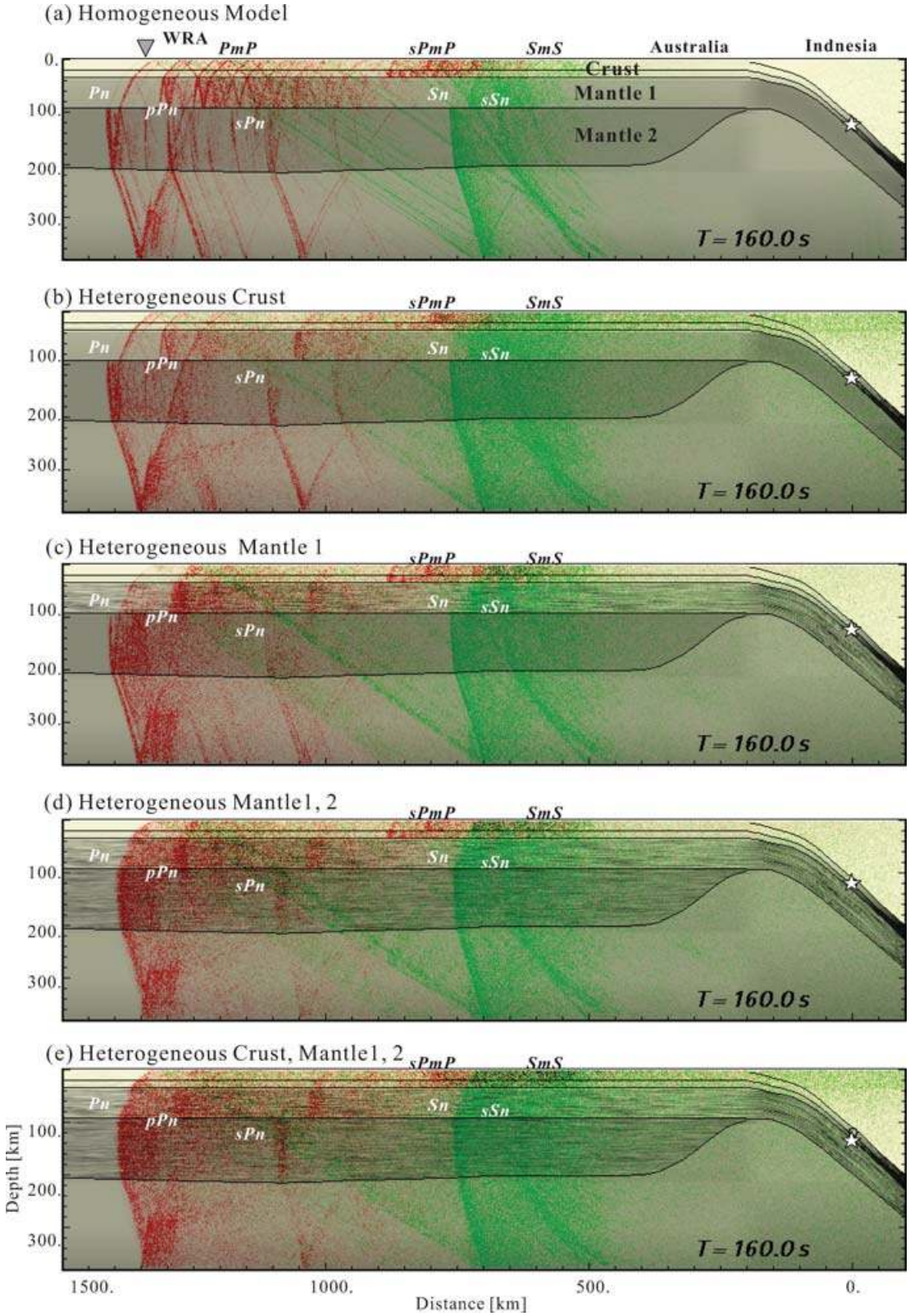

Figure 13. Snapshots of the seismic wavefield for different class of heterogeneities in the lithospheric crust and mantle. (a) homogeneous crust and mantle layers, including heterogeneities; (b) in the crust, (c) in the mantle, (d) in the mantle1 and mantle2 layers and (e) throughout the crust and mantle 1, 2.

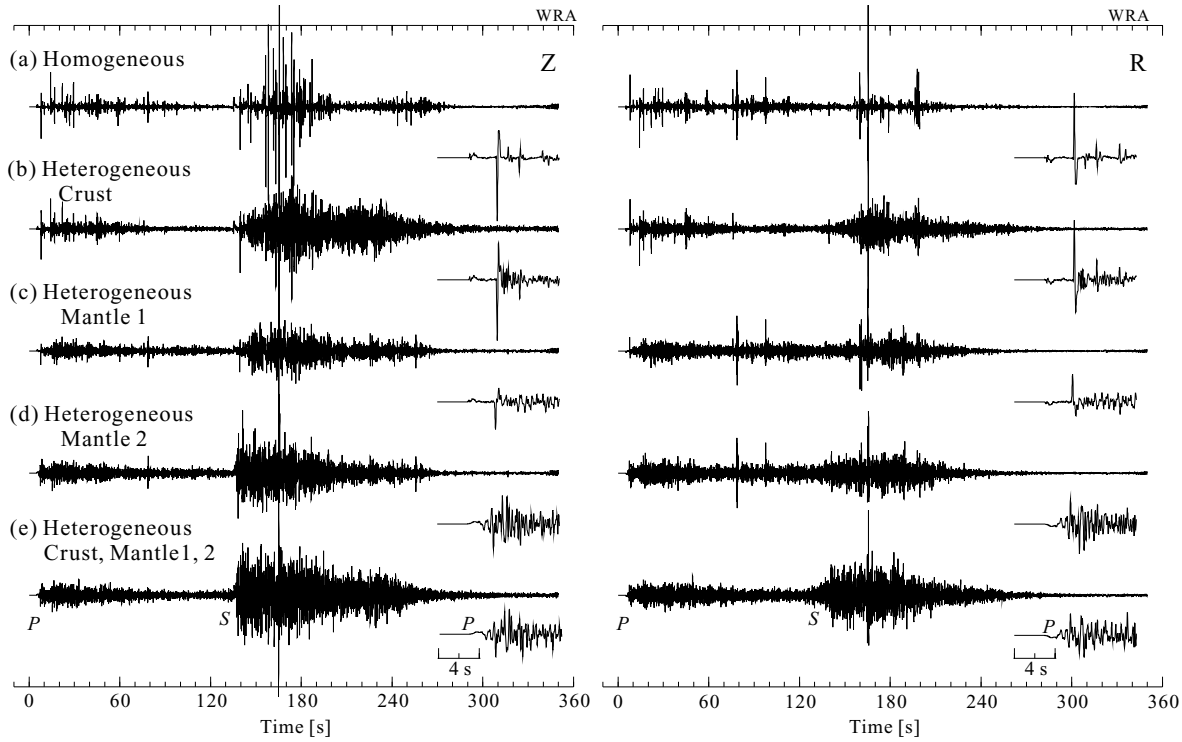

Figure 14. Synthetic seismograms for the radial and vertical components of ground velocity at WRA comparing the change in wave shape as the distribution of heterogeneities in the crust and mantle change. An expansion of the P wave onset is shown at the right-hand end of each trace.

produces only slightly enhanced P and S waves with some extension of the coda.

When the heterogeneous zone in model (d) is extended to include both the regions mantle1 and mantle2 and so continue to a depth of 210 km and total thickness of 175 km, the simulation results show a remarkably large and sharp Sn phase and with long S-wave coda following (Fig. 14d). The snapshots of seismic wavefield shown in Fig. 13(d) demonstrate that there is a thick band of P- and S-wave energy trapped within the deeper part of the mantle lithosphere below the Australian craton. Moreover the simulated waveform demonstrates a clear separation of low- and high-frequency signals with a time interval of 1–2 s that was not well reproduced in the previous models with a thinner quasi-lamina region.

The synthetic seismogram in Fig. 14(d) shows somewhat artificial reflections between P and S waves and relatively larger P wave coda in the radial-component seismogram. Such anomalous patterns of reflection are suppressed by introducing random heterogeneities throughout the crust and the full mantle structure in model (e) to produce strong seismic scattering within a thick heterogeneous lithosphere (Figs 13e and 14e). The distribution of scatterers through the full thickness of the Australian lithosphere enhances the amplitude of the P- and S-wave coda significantly with a similar amplitude level for horizontal and vertical motions as seen in the observations.

3.3 Effect of the shape of heterogeneities

The quasi-lamina structure described by aeolotropic properties of a stochastic random distribution of elastic properties in the thick Australian lithosphere can support an effective scattering waveguide process for high-frequency seismic signals. Similar behaviour has already been shown in a range of 2-D and 3-D numerical simulations for subduction zone earthquakes in Japan (Furumura & Kennett 2005).

We now conduct an additional set of simulations to examine how the character of the random heterogeneities in the lithosphere influences the trapping of high-frequency seismic waves in the lithosphere as they propagate from the subduction zone source. In this group of experiments the correlation properties and the amplitude of heterogeneities in the crust and mantle have been varied for the same basic lithosphere model.

The first model assumes isotropic stochastic media sharing identical statistics for the elastic parameter distribution (standard deviation of 2 per cent in the crust and mantle1 and 1 per cent in the mantle2) and effective area of scatterers ($A_x = A_z = 1.2$ km in the crust and 3.2 km in the mantle). A snapshot at 160 s is shown in Fig. 15(a), and synthetic seismograms of radial and vertical motion for the WRA site (as marked in Fig. 15a) are displayed in Fig. 16(a). Isotropic scatters in the lithosphere produce strong scattering of high-frequency signals and so there is a long coda in P and S waves. However, the leakage of high-frequency seismic energy from the heterogeneous lithosphere into the deeper mantle is very striking, and the attenuation of the seismic waves is significant as time progresses. Moreover, the scattering from such an isotropic scattering distribution does not show the separation of the low-frequency precursor and the high-frequency later arrivals for the Pn signals, even though this is prominent in the results above for elongated scatterers (Figs 14b–e). Thus, a model with isotropic scatterers in the lithosphere produces a similar level of scattering and high-frequency coda, but is not sufficient to keep a high-frequency seismic signal propagating for long distances within the lithosphere.

As the aspect ratio of the random scatterers increases as shown in Figs 15(b) and 16(b) ($A_x = 20$ km, $A_z = 0.5$ km in the crust and $A_x = 5$ km, $A_z = 0.25$ km in the crust) large P- and S-wave coda very quickly develop, and the synthetic seismograms for radial and

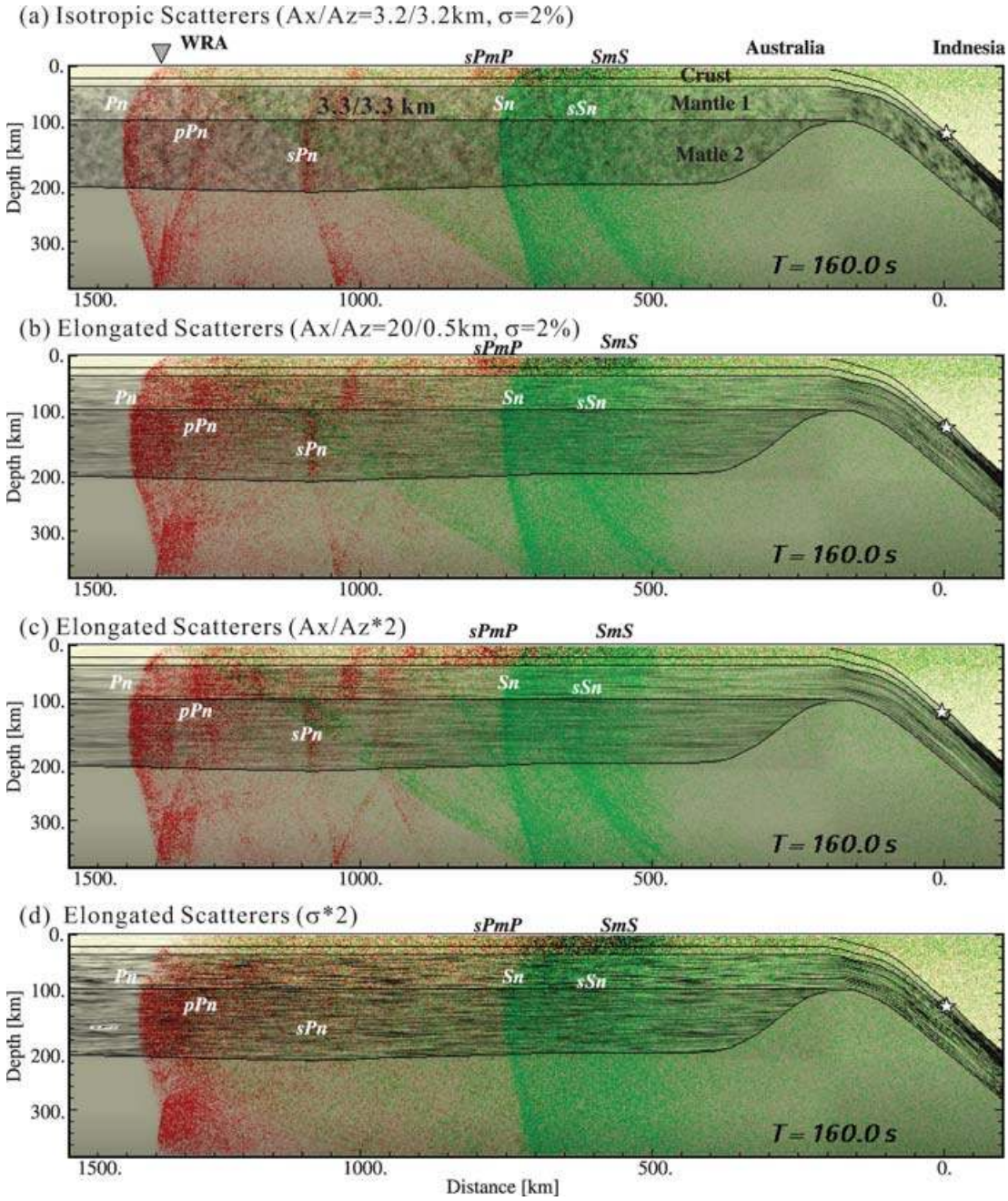

Figure 15. Snapshots of the seismic wavefield at 160 s for models with different distributions of random heterogeneities: (a) isotropic scatterers, (b) horizontally elongated anisotropic scatterers, (c) enhanced aspect ratio of elongated scatterers and (d) increased amplitude of heterogeneity.

vertical motions show a similar pattern of slow decay of high-frequency coda to that for seismograms in the Australian lithosphere from Indonesian subduction zone earthquakes. The separation of low-and high-frequency later signals occurs for this class of quasi-lamina structure and the offset time between low- to high-frequency signals of about 2 s is almost comparable to the observations. The offset time and coda shape of P and S waves are significantly modified as the aspect ratio of elongated heterogeneity increases, but the waveform of the high-frequency wavefield is rather insensitive to the scale of heterogeneity as specified by the correlation distance (Figs 15c and 16c).

We have also examined the change in the waveforms as the level of random fluctuation is increased (to $\sigma = 4$ per cent) from the scenario in the base model, but retaining the same elastic properties. The resulting seismic wavefield and the seismograms at WRA are shown in Figs 15(d) and 16(d) for the higher level of fluctuations. There is now a significant elongation of the high-frequency P- and S-wave coda with very long time separation between low- to high-frequency signals of more than 4 s. The synthetic seismograms show an unusual shape of waveforms with an unclear onset of the S-wave signal and a spindle shape for the S-wave coda, which is inconsistent with the observed seismograms in northern Australia from the subduction zone sources.

Thus the comparison between the set of simulations for different random heterogeneity model and the observations indicates that the heterogeneity level in the Australian lithosphere for the 2-D model

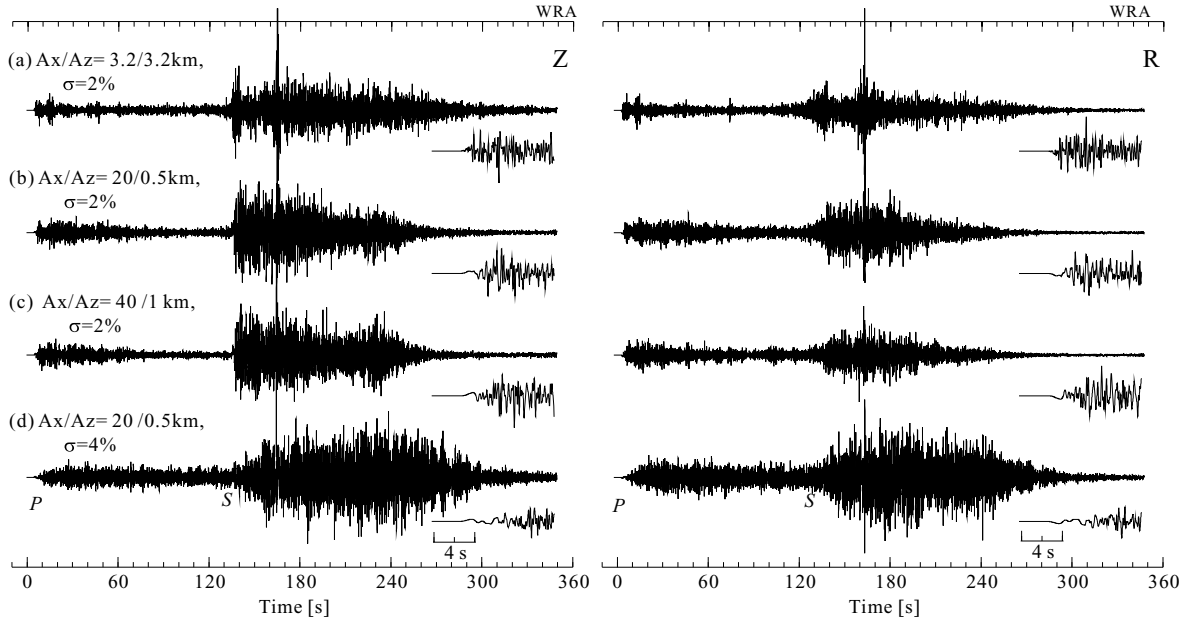

Figure 16. Synthetic seismograms for the radial and vertical components of ground velocity at the WRA epicentral distance, comparing the changes in wave shape as the properties of the heterogeneities in the model are varied: (a)–(d) correspond to the models shown in Fig. 15.

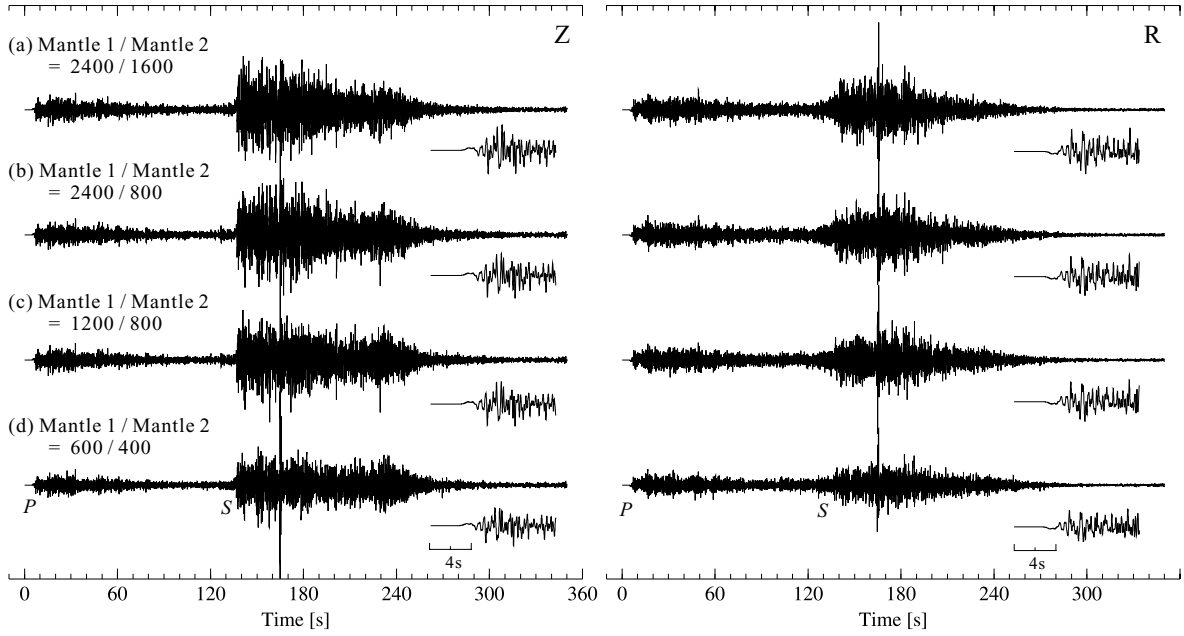

Figure 17. Synthetic seismograms for the radial and vertical components of ground velocity at WRA comparing the changes in wave shape associated with modifications of the anelastic attenuation (Q_p) structure in the mantle (Mantle1, Mantle2).

is well described with a standard deviation of 2 per cent and should not be significantly increased.

3.4 Effect of mantle *Q*

The high intrinsic Q in the stable Australian lithosphere is also likely to be an important contributor to the processes retaining high-frequency P- and S-wave energy within the quasi-laminated structure over very long propagation distances of more than 1000 km from the subduction zone. In the previous simulation we used rather large Q ($Q_p = 600$–1600; $Q_s = Q_p/2$) values in the crust and mantle structure, based on the analysis of Gudmundsson et al. (1994).

We here examine the sensitivity of the guiding of high frequency signals to the intrinsic attenuation properties (Q_p and Q_s) of the Australian lithosphere. Synthetic seismograms of the radial and vertical components of ground velocity derived from models with increased attenuation (lowered Q) in the crust and mantle structure are compared in Fig. 17 for a common station WRA for the source depth of 120 km. The attenuation coefficient for P waves (Q_p) in Mantle1 and Mantle2 for each model are indicated in the figure and the shear wave Q_s is assumed to be half of the value for Q_p($Q_s = Q_p/2$).

The simulation results indicate that the overall character of the wavetrain, such as the amplitude of the Pn and Sn phase and the following long coda waves, are rather insensitive to the specific Q

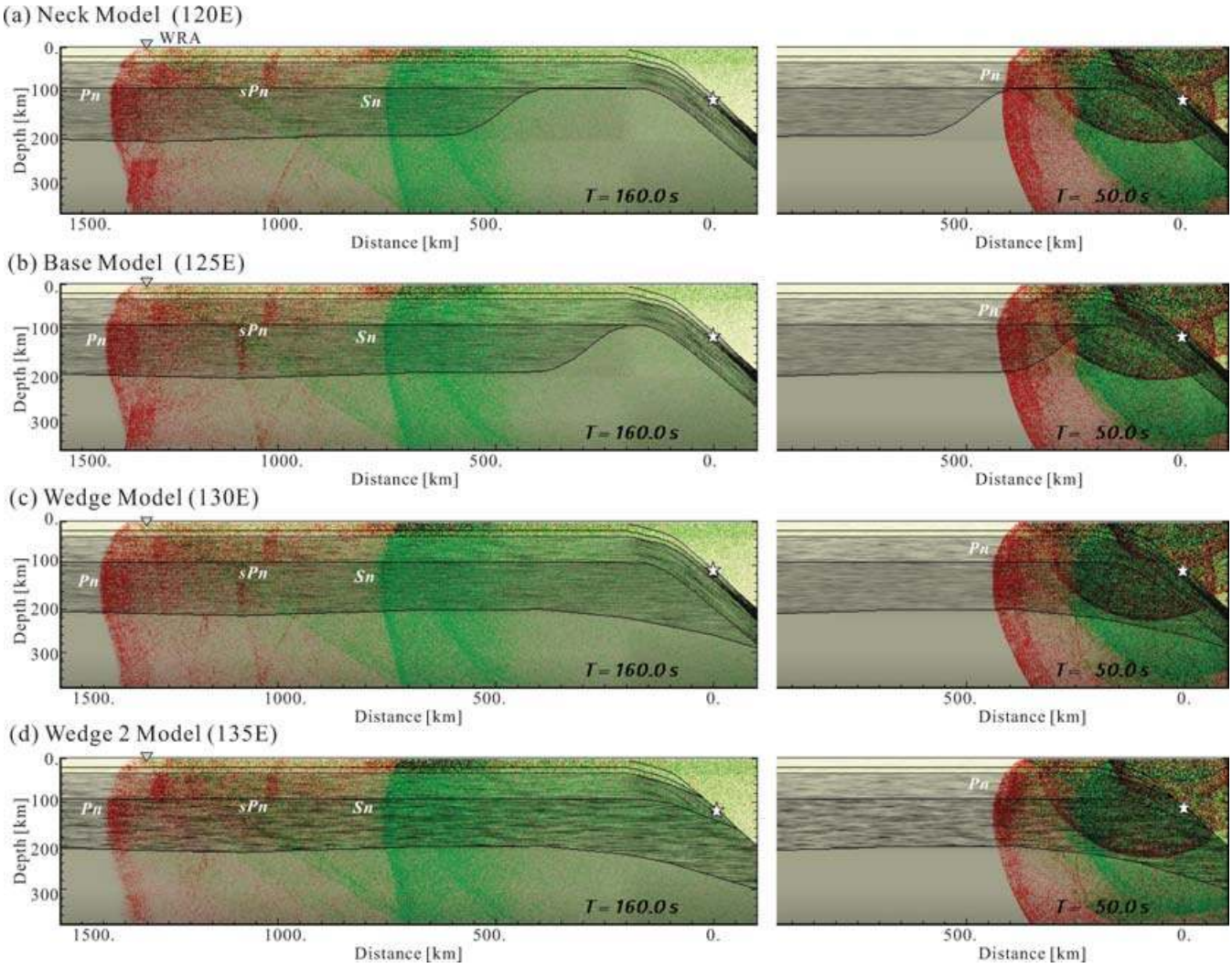

Figure 18. Snapshots of seismic wave propagation at T = 50 and 160 s after earthquake initiation for different class of subduction zone structural models (a)–(d) with a common source at 120 km depth.

values in the mantle, especially in the deeper part of the lithospheric mantle (Mantle2). With rather low Q values assigned entirely to the mantle, the simulated waveform still persists with very long coda for P and S waves. This indicates the significant role played by crustal scattering. The strong internal scattering of seismic signals within the thick continental lithosphere is the main cause for the high-frequency stochastic waveguide in the Australian lithosphere and is helped by the high intrinsic Q values in continental structure.

3.5 Effect of subduction zone structure

The model employed so far for the simulation has a smooth transition between the thick Australian lithosphere and the subducting slab beneath Indonesia. In such a structure we can expect relatively smooth guiding of seismic waves into Australian lithosphere from the source in the subducting plate.

However, the structure of the subduction zone varies along the arc as illustrated in Fig. 7, which is derived from the high-resolution tomographic model of Widiyantoro & van der Hilst (1997), and thus we need to examine the effect of shape of the transition structure on the transmission of seismic energy from the subduction zone into the Australian cratonic lithosphere. We have therefore prepared a group of models designed to capture the major features of the structure revealed by the tomography. The models and associated simulations are illustrated in Fig. 18.

For the western part of the arc (zone A-120E in Fig. 7), the thick continental lithosphere has not reached the subduction zone and so there is a long 'neck' of oceanic lithosphere bridging to the subduction zone. This 'neck' model is shown in Fig. 18(a) with snapshots of the seismic wavefield for time windows at T = 50 and 160 s after source initiation, which are to be compared with the results from the 'base' transmission model (repeated as Fig. 18b).

In the earlier (T = 50 s) time frame we see is a dramatic escape of seismic energy into deeper mantle from the thin oceanic lithosphere segment and only a small portion of such energy returns from the mantle into the Australian lithosphere. There are weak Pn and Sn signals travelling in the Australian lithosphere that can be seen in the snapshot for the later time frame (160 s), especially in weak sPn signals in the Mantle2 region. The corresponding synthetic seismograms for this model (Fig. 19a), at the WRA marker, show weak P and S signals on both vertical and radial component. The coda has a generally similar character to that for the base model, but for this neck model the energy peak is shifted later in the S-wave segment.

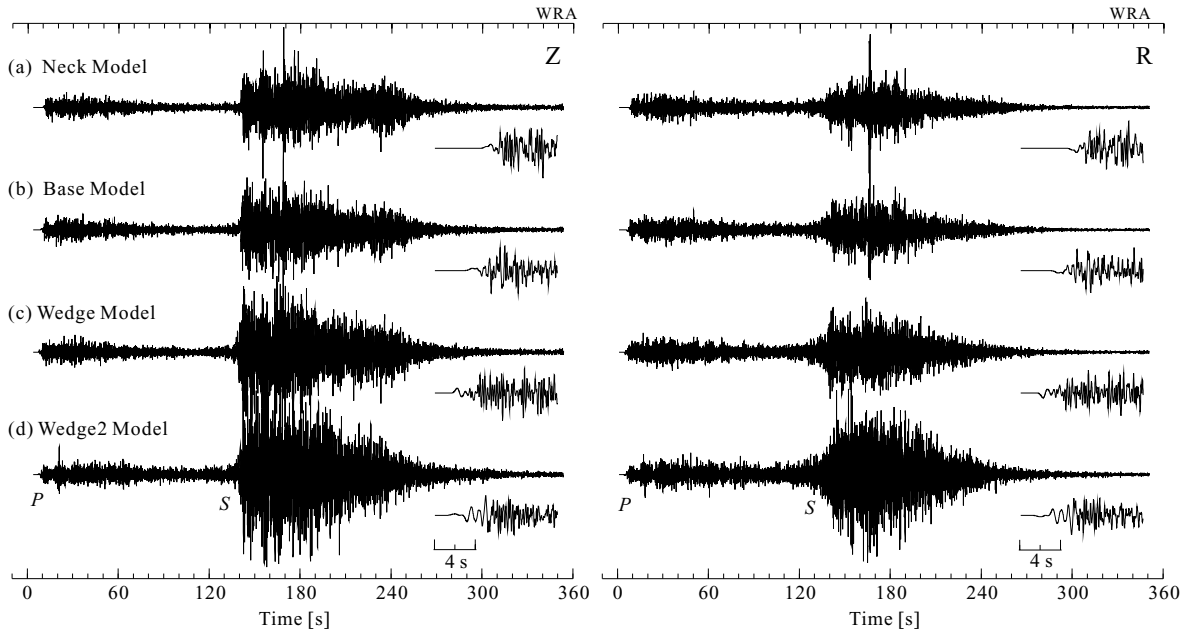

Figure 19. Synthetic seismograms for a receiver at WRA illustrating the change in the wave shape as the nature of the transition zone between the subduction zone and the Australian lithosphere changes for model (a)–(d); see Fig. 7.

Further to the east (zone C, 128E) the thick Australian lithosphere has reached the trench and subduction has ceased, and even further east the continental lithosphere appears to directly descend below the trench (zone D, 131E). We model these variations in structure with a thickened mantle structure in the transition zone as illustrated in Fig. 18(c) ('wedge' model), and Fig. 18(d) ('wedge2' model). The snapshots of seismic wavefield for the two wedge models (Figs 18c and d) illustrate the efficient transmission of seismic energy from a 120-km-deep source into the Australian lithosphere, the coupling into the continental lithosphere is most effective when the former oceanic lithosphere has been displaced (Fig. 18d). For both of the 'wedge' models there are large Pn and Sn signals with extensive following coda (Figs 18c and d), but only weak P- and S-wave energy leaking into the surrounding mantle from the source. The corresponding synthetic seismograms for these wedge models (Figs 19c and d) show very large amplitudes, and a long duration of P- and S-wave coda with slower decay than for the base or neck models.

The nature of the structure connecting the subduction zone to the thick Australian cratonic lithosphere plays very important role in the transmission of seismic energy into the continental lithosphere through the particular characteristics of the P and S phases and their coda. The differences between the various models are comparable to those seen in observations from sources at different places along the Indonesian arc. In particular events from the east show a stronger coda with less rapid decay (Fig. 1) than for events in the western segment (Fig. 5).

4 DISCUSSIONS AND CONCLUSIONS

We have been able to show that the complex patterns of high-frequency wave propagation observed at stations in northern Australia for subduction zones source in the Indonesian arc can be well represented by models with distributed aeolotropic heterogeneity through the lithosphere. The specific configuration of the continental lithosphere relative to the subduction zone modifies the details of the wavefield in ways that correspond to the variations in the observed seismograms. In all cases we need a combination of crustal and mantle heterogeneity, with much longer horizontal correlation length than vertical, to provide a satisfactory representation for the nature and duration of the P- and S-wave codas. The character of the observed field does not show any obvious directional dependence on the azimuth of propagation relative to the normal to the subduction zone, so that there is no evidence for a preferred orientation of the scattering components in the horizontal plane.

In order to simulate very long distance propagation at high frequencies we have had to use 2-D models. This means that we cannot include out-of-plane scattering that clearly contributes significantly to the observations, with clear tangential components to the P-wave coda. We have therefore undertaken a comparison of 3-D and 2-D models outlined in Appendix A, to examine the way in which the simplified propagation model might lead to misinterpretation. Encouragingly, apart from the out-of-plane component, it would appear that the general character and properties of the wavefield are well reproduced. There are conflicting tendencies, the amplitude of the scattered field may be underestimated by a 2-D calculation for a given heterogeneity level, but the duration of the coda is likely to be longer because energy is confined to a plane. Overall this means that there may be a slight over-estimate of the necessary level of heterogeneity when we use a 2-D simulation to understand 3-D variations. It will be some time before the computational resources are available to undertake 3-D simulations for the high frequencies and long propagation paths used in this study.

Fuchs & Schulz (1976) appear to have been the first to suggest a quasi-laminated structure in the upper mantle as a means of understanding the differences in character between the lower and higher frequency parts of the wavefield for long distance P-wave propagation. The ideas have been applied extensively to studies of the data from long-range refraction experiments in the former Soviet Union using nuclear sources (e.g. Morozova et al. 1999). There has been considerable debate on the relative importance of the crustal and mantle components of heterogeneity needed to produce the long-range propagation of high-frequency Pn and Sn signals with

long tails based on differing styles of computer simulation (e.g. Morozova *et al.* 1999; Tittgemeyer *et al.* 1999, 2000; Nielsen & Thybo 2003; Ryberg *et al.* 2000).

As can be seen from Figs 13 and 14, scattering in the crust is important but to match the extensive Australian observations for earthquakes sources we must have some significant component of mantle heterogeneity as well. The correlation length in the mantle lithosphere is much longer than for the crust. The present models have been built on our earlier results for stochastic wave guides in subduction zones (Furumura & Kennett 2005) and show how the high frequency energy can be injected from the subduction zone into the continental lithosphere. We have looked at a range of models and found a set of parameters that provide a good match to the observations, but have not explored more than a small fraction of possible heterogeneous structures. In particular, the details of depth variation and gradations in correlation properties are not strongly constrained by the nature of the seismic observations.

Nevertheless the results suggest that the smaller scale heterogeneity in the lithosphere is organized with aeolotropic correlation properties with scale lengths of the order of tens of kilometres, both in the oceanic lithosphere entering subduction zones and in the continental cratonic lithosphere. Such organization with longer horizontal scales than vertical appears to represent an intrinsic property of the lithosphere that is presumably related to the way it is formed and subsequently modified. We now face the challenge of understanding the nature of the small-scale variability.

ACKNOWLEDGMENTS

The deployments of portable broad-band instruments across Australia and subsequent data extraction have involved many members of the Seismology Group at the Research School of Earth Sciences, Australian National University since 1992 and all are thanked. We also thank Agus Abdulah for the differential attenuation measurements reported in Fig. 6.

REFERENCES

Cerjan, C., Kosloff, D., Kosloff, R. & Reshef, M., 1985. A nonreflecting boundary condition for discrete acoustic and elastic wave equations, *Geophysics*, **50**, 705–708.

Fishwick, S., Kennett, B.L.N. & Reading, A.M., 2005. Contrasts in lithospheric structure within the Australian Craton, *Earth planet. Sci. Lett.*, **231**, 163–176.

Furumura, T. & Chen, L., 2004. Large scale parallel simulation and visualization of 3-D seismic wavefield using the Earth Simulator, *Comput. Model. Eng. Sci.*, **6**, 153–168.

Furumura, T. & Kennett, B.L.N., 2005. Subduction zone guided waves and the heterogeneity structure of the subducted plate—intensity anomalies in northern Japan, *J. geophys. Res.*, **110**, B10302, doi:10.129/2004JB003486.

Furumura, T. & Kennett, B.L.N., 2008. A scattering waveguide in the heterogeneous subducting plate, in *Advances in Geophysics: Scattering of Short-Period Seismic Waves in Earth Heterogeneity*, eds Sato, H. & Fehler, M., Elsevier, Amsterdam.

Fuchs, K. & Schulz, K., 1976. Tunneling of low-frequency waves through the subcrustal lithosphere, *J. Geophys.*, **42**, 175–190.

Gudmundsson, O., Kennett, B.L.N. & Goody, A., 1994. Broadband observations of upper mantle seismic phases in northern Australia and the attenuation structure in the upper mantle, *Phys. Earth planet Inter.*, **84**, 207–226.

Hong, T. & Wu, R.S., 2005. Scattering of elastic waves in geometrically anisotropic random media and its implication to sounding of heterogeneity in the Earth's deep interior, *Geophys. J. Int.*, **163**, 324–338.

Kaiho, Y. & Kennett, B.L.N., 2000. Three-dimensional seismic structure beneath the Australasian region from refracted wave observations, *Geophys J. Int.*, **142**, 651–668.

Kennett, B.L.N., 1983. *Seismic Wave Propagation in Stratified Media*, Cambridge University Press, Cambridge.

Kennett, B.L.N., 1986. On regional S waves, *Bull. seism. Soc. Am.*, **75**, 1077–1086.

Kennett, B.L.N., 1987. Observational and theoretical constraints on crustal and mantle heterogeneity, *Phys. Earth planet. Inter.*, **47**, 319–322.

Kennett, B.L.N., Engdahl, E.R. & Buland, R., 1995. Constraints on the velocity structure in the Earth from travel times, *Geophys. J. Int.*, **122**, 108–124.

Korn, M., 1988. P-wave coda analysis of short-period array data and the scattering and absorptive properties of the lithosphere, *Geophys. J. Int.*, **93**, 437–449.

Morozova, E.A., Morozov, I.B., Smithson, S.B. & Solodilov, L.N., 1999. Heterogeneity of the uppermost mantle beneath Russian Eurasia from the ultra-long range profile QUARTZ, *Geophys. Res. Lett.*, **104**, 20 329–20 348.

Nielsen, L. & Thybo, H., 2003. The origin of teleseismic Pn waves: multiple scattering of upper mantle whispering gallery phases, *J. geophys. Res.*, **108**, 2460, doi:10.1029/2003JB002487.

Nielsen, L., Thybo, H., Levander, A. & Solodilov, N., 2003. Origin of upper-mantle seismic scattering—evidence from Russian peaceful nuclear explosion data, *Geophys. J. Int.*, **154**, 196–204.

Robertsson, J.O.A., Blanch, J.O. & Symes, W.W., 1994. Viscoelastic finite-difference modeling, *Geophysics*, **59**, 1444–1456.

Ryberg, T., Tittgemeyer, M. & Wenzel, F., 2000. Finite-difference modelling of P-wave scattering in the upper mantle, *Geophys, J. Int.*, **141**, 787–800.

Saito, T., 2006. Synthesis of scalar-wave envelopes in two-dimensional weakly anisotropic random media by using the Markov approximation, *Geophys. J. Int.*, **165**, 501–515.

Tittgemeyer, M., Wenzel, F., Ryberg, T. & Fuchs, K., 1999. Scales of heterogeneities in the continental crust and upper mantle, *Pure appl. Geophys.*, **156**, 29–52.

Tittgemeyer, M., Wenzel, F. & Fuchs, K., 2000. On the nature of Pn, *J. geophys. Res.*, **105**, 16 173–16 180.

Widiyantoro, S. & van der Hilst, R.D., 1996. Structure and evolution of Lithospheric Slab beneath the Sunda arc, Indonesia, *Science*, **271**, 1566–1570.

Xie, J. & Nuttli, O., 1988. Interpretation of high frequency coda at large distances: stochastic modelling and method of inversion, *Geophys. J. Int.*, **93**, 579–595.

APPENDIX A: 2-D AND 3-D SCATTERING WAVEFIELDS

Our simulation results are for 2-D models and thus account only for the scattering effects in the in-plane direction, and miss the

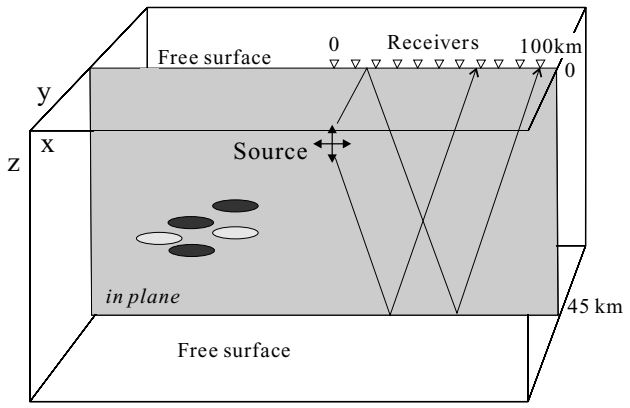

Figure A1. Model configuration for 3-D and 2-D FDM simulation for a stochastic random heterogeneous model. Configuration of source and receivers are illustrated.

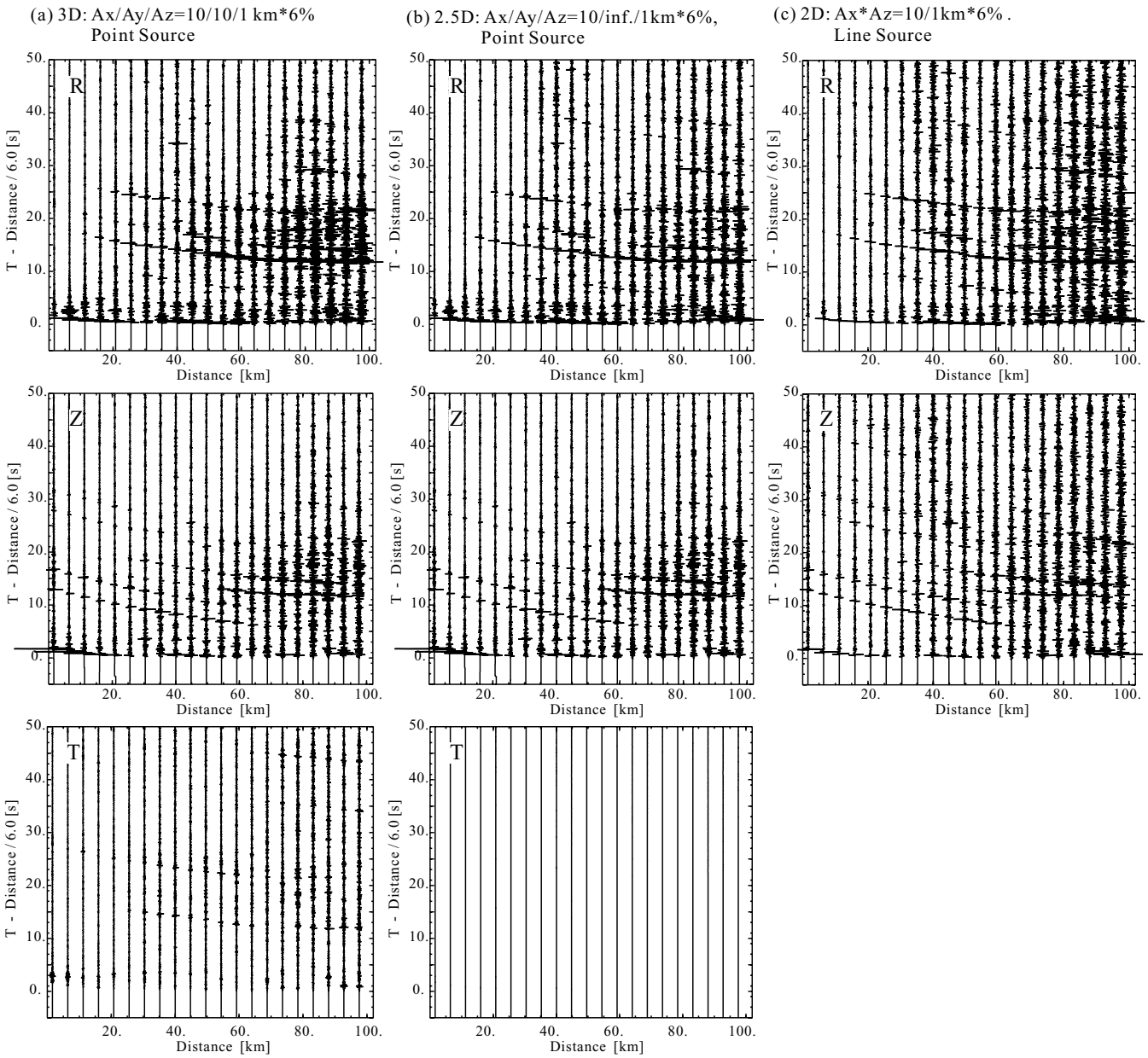

Figure A2. Synthetic seismograms of radial (R), vertical (Z) and transverse (T) components of velocity derived from (a) 3-D simulation model with stochastic random heterogeneities and a point source (b) 2.5-D modelling assuming that model parameters are invariant in out-of-plane (tangential) direction and a point source and (c) 2-D simulation using the same structure as (b) but for a line source.

effect of out-of-plane scattering, that is clearly evident in the observations though, for example, P coda on the transverse component. In addition, the source model employed in the 2-D FDM simulation assumes a line source extending infinitely in the out-of-plane direction, and so the wave shape and geometrical spreading will be different to that for a point source in 3-D. Other theoretical studies of 2-D scattering with anisotropic correlation functions have been carried out by Hong & Wu (2005) and Saito (2006), but again have not addressed the influence of the third dimension.

To examine the influence of the 2-D approximations needed to secure long-range propagation at high frequencies, we have carried out a full 3-D FDM simulation of the scattering of seismic waves using the Earth Simulator supercomputer.

A1 Simulation model

The 3-D model covers a zone 204.8 km × 204.8 km × 45 km in depth, which has been discretized with a uniform grid increment of 0.1 km × 0.1 km × 0.05 km into a 4.3×10^9 gridpoint model (Fig. A1). We use a simple half-space model with an average P wave speed $V_p = 6.0$ km s^{-1}, S wave speed $V_s = 3.5$ km s^{-1} and density $\rho = 2.6$ t m^{-3}. The 45-km-thick model has free surface conditions at top and bottom. An absorbing boundary (Cerjan et al. 1985) is introduced in a zone 40 gridpoints wide surrounding the 3-D model in order to suppress artificial reflections from the model boundaries. Stochastic heterogeneities are introduced throughout the half-space model with a correlation length of $A_x = A_y = 10$ km in the horizontal directions and a smaller correlation length

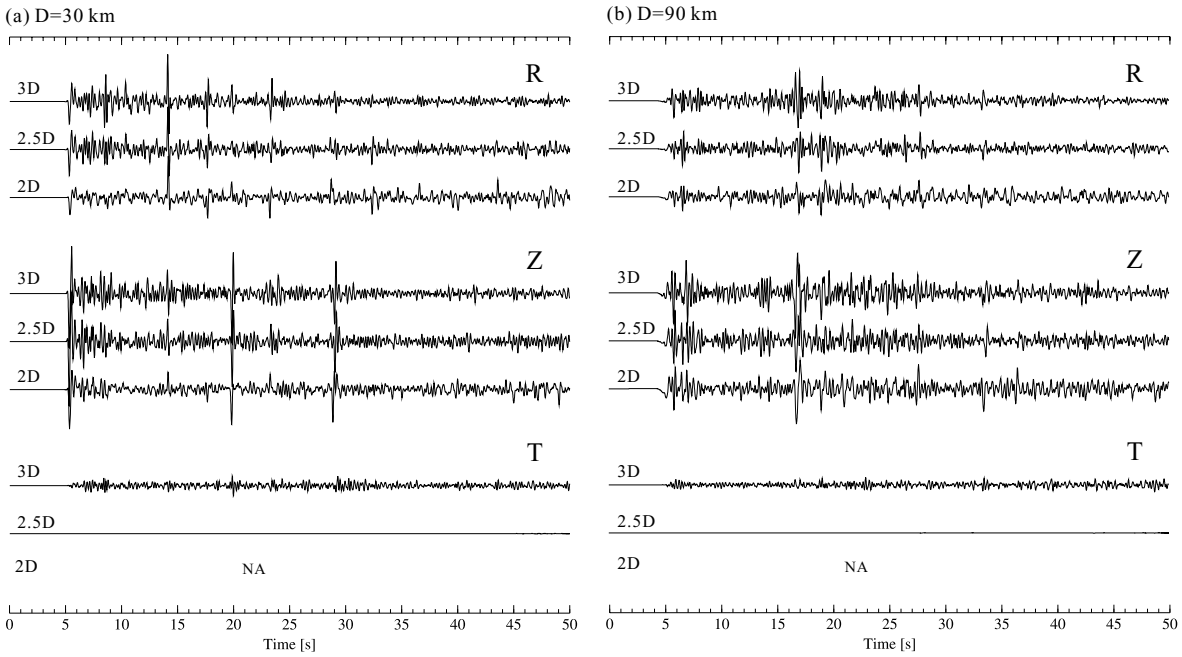

Figure A3. Expanded seismograms of Fig. A2 comparing the waveforms and decay rate of synthetic seismograms from 3-D, 2.5-D and 2-D simulations for fixed propagation distance, (a) 30 km and (b) 90 km.

$A_z = 1$ km in vertical direction. The standard deviation of the fluctuations for V_p, V_s and ρ are $\sigma = 6$ per cent from the background model. Such strong heterogeneity will produce significant scattering effects for the limited spatial dimensions of this model, even though the largest available distance is somewhat smaller than for typical lithospheric propagation.

As in the main calculations, a parallel FDM method for the full elastic problem was used with an accurate 16th-order staggered grid in the horizontal direction and a conventional fourth-order FDM in vertical direction. With a minimum shear wave velocity of stochastic random heterogeneity model of $V_s = 3.29$ km s^{-1} and a grid size of 0.1 km in the higher-order FDM simulation, we can simulate seismic wave propagation for frequencies up to 5 Hz with a sampling of 5.48 gridpoints per wavelength for the highest frequencies in the horizontal directions and 10.96 gridpoints in the vertical direction. We use weak intrinsic attenuation ($Q_p = 2400$, $Q_s = 1200$) in the model to enhance the scattering of high-frequency signals caused by strong heterogeneities in the model.

An explosive source is placed in the centre of the model at depth of $h = 11.25$ km from the upper free surface, which radiates high-frequency P waves isotropically into the 3-D model. The 3-D FDM simulation is conducted by parallel computing using 128 node (1024 vector processors) of the Earth Simulator, with computer memory of 0.86 Tbyte and CPU time of 3.4 hr to calculate wave propagation over an interval of 90 s with using over 30 000 time steps.

A2 Simulation result

The results of the 3-D simulations are shown in Fig. A2(a) with synthetic seismograms of three-component ground motions for a set of stations in a line along the x-direction. For comparison in Fig. A2(b) we show the results for a 2-D heterogeneity mode where the properties of the model are invariant in the horizontal (y) direction (e.g. 2.5-D wavefield). A 2-D simulation of the radial and vertical ground motions in a model taken from the vertical plane through the source for the 3-D case is shown in Fig. A2(c). A high-cut filter with a cut-off frequency of 5 Hz is applied to the synthetic seismograms to reduce the influence of numerical dispersion which has different character in the 2-D and 3-D FDM calculations.

The synthetic seismograms of three-component ground motions (Z, R and T components) for the 3-D and 2-D simulations are illustrated in Fig. A2. Details of the seismograms at distances of 30 and 90 km are shown in Fig. A3; each trace is multiplied by the epicentral distance to roughly compensate for geometrical spreading. Multiple reflections of P waves between the free surfaces at the top and the bottom of the model, with a time separation of about 10 s, are very clear. The reflection processes allow an effective continuation of the wavefield to a larger domain and contribute to the higher frequency scattering.

Comparison of the waveforms for the different simulations shows good correlation between scattering wavefield derived from the 2.5-D and 3-D FDM results, particularly for characteristics of the P and PS converted signals and long coda of high-frequency signals in both radial and vertical component ground motions. However, the amplitude of coda at most stations is a little lower for the 2.5-D wavefield and decay rate of coda somewhat quicker. This arises because strong scattering of seismic wavefield in the out-of-plane direction is not accounted for in such a 2.5-D model. This 3-D scattering effect would be more significant with stronger horizontal heterogeneities, but it is rather mild in the present model with relatively large correlation length and the same scale in the two horizontal directions ($A_x = A_y = 10$ km).

The relatively large amplitude of the tangential-component ground motion for the 3-D simulation indicates strong scattering of P waves, which will remove some P-wave energy from the main arrivals for the in-plane motion. The energy of tangential motions increases gradually with increasing time as waves propagating through the heterogeneous structure, so that the discrepancy between 3-D and 2.5-D wavefields increases with increasing epicentral distance.

Such tangential energy arising from out-of-plane scattering should not appear in the 2.5 D model, and we see no seismic signals from the simulation, confirming the accuracy of the 3-D calculations.

The synthetic seismograms from the 2-D calculation show a similar character to the 2.5-D wavefield both have same in-plane structure and are invariant in the out-of-plane direction, but the dominant period of the 2-D seismic waves produced by a line source is slightly longer than for 2.5-D and 3-D wavefield of the point source. Moreover, the decay rate of a line source in 2-D as a function of distance R is given by $R^{-1/2}$ and so is weaker than the R^{-1} expected for a point source in 3-D. The result is an apparent development of a longer coda in the 2-D simulation since the later arrivals at larger propagation distances do not attenuate so quickly.

The results of these computer simulations demonstrate that the 2-D model used in this study is well suited to describe the main characteristics of the scattering wavefield in 3-D, even though out-of-plane scattering is excluded. The weaker geometrical spreading in 2-D tends to compensate for this effect.